Gondwana Research 153 (2026) 344–361

Contents lists available at ScienceDirect

Gondwana Research

journal homepage: www.elsevier.com/locate/gr

Research Paper

Late Paleozoic-Mesozoic uplift, exhumation, and burial of southern Gondwana margin: Thermochronological and stratigraphic constrains from Victoria Land (Antarctica)

Valerio Olivetti [a,*], Luca Zurli [b,c], Silvia Cattò [a], Fabrizio Balsamo [d], Gianluca Cornamusini [b,c], Marco Fioraso [b], Matteo Perotti [b], Giorgia Guzzo [a], Massimiliano Zattin [a], Federico Rossetti [e]

[a] *Department of Geosciences, University of Padova, Padova, Italy*
[b] *Department of Physical, Earth and Environmental Sciences, University of Siena, Siena, Italy*
[c] *National Museum of Antarctica – Siena Section, University of Siena, Siena, Italy*
[d] *Department of Chemistry, Life Sciences and Environmental Sustainability, University of Parma, Parma, Italy*
[e] *Department of Science, University of Roma Tre, Rome, Italy*

A R T I C L E I N F O

Keywords:
Transantarctic Basin
Beacon Supergroup
Zircon (U-Th)/He dating with variable eU content
Apatite fission-track thermochronology
Antarctica

A B S T R A C T

The late Paleozoic-Mesozoic geological record of Antarctica is preserved in sedimentary successions deposited in the Gondwanide retroarc foreland basin. This basin developed as a direct response to convergence and crustal thickening along the southern margin of Gondwana during subduction of the paleo-Pacific plate. This protracted convergent tectonic setting drove the evolution of the Transantarctic Basin, which persisted from the Devonian through the Jurassic. The Transantarctic Basin is primary filled up by continental deposits, now exposed along the Transantarctic Mountains from the Weddell Sea to the northern Victoria Land. These Devonian-Jurassic sedimentary successions exhibit variations in thickness, provenance, and sedimentary facies, reflecting the long-term evolution of the paleo-Pacific convergent margin. This study investigated the late Paleozoic-Mesozoic paleo-topographic evolution of the central Prince Albert Mountains, where a thin Gondwanan stratigraphic succession is exposed. We integrate low-temperature thermochronological data (apatite fission-track and zircon (U-Th)/He) with stratigraphic evidence. Modeled thermal histories reveal an exhumation episode during the late Carboniferous to Permian, associated with the growth and subsequent erosion of a previously undescribed topographic high, referred to as Prince Albert High. The Prince Albert High formed between northern and southern Victoria Land and evolved synchronously with the Devonian-Triassic deposition of the Beacon Supergroup. We interpret its formation as a response to far-field stresses transmitted from the paleo-Pacific convergent margin, providing new insights into the geodynamic history of the Transantarctic Basin. Subsequently, this topographic high was buried beneath a Mesozoic overburden. This burial left evidence of a medium-temperature (150–180 °C) reheating process recorded in the basement and cover rocks.

1. Introduction

The Transantarctic Basin is a long-lived continental basin system that developed over approximately 200 Myr, from the Devonian to the Early Jurassic, along the paleo-Pacific margin of Gondwana (Isbell 1999; Elliot, 2013 and references therein). Its formation began atop a peneplaned surface, known as the Kukri Erosion Surface (Gunn and Warren, 1962; McKelvey et al., 1977; Isbell, 1999). This extensive, flat surface was created by the prolonged erosion of the underlying Neoproterozoic to Ordovician Ross Orogen (Goodge, 2020).The siliciclastic succession of the Beacon Supergroup (Devonian to Jurassic), now widely exposed throughout the Transantarctic Mountains (TAM) (Fig. 1a), records the prolonged history of depositional infill within the Transantarctic Basin (Barrett, 1981; 1991; Goodge 2020).

The geodynamic context of the Transantarctic Basin remains ambiguous due to uncertainties regarding its spatial and temporal

* Corresponding author.
E-mail address: valerio.olivetti@unipd.it (V. Olivetti).

https://doi.org/10.1016/j.gr.2025.12.003
Received 26 March 2024; Received in revised form 23 November 2025; Accepted 2 December 2025
Available online 31 December 2025
1342-937X/

relationships with the paleo-Pacific margin, as well as the space–time variability in basin geometry, paleo-topography, and sediment provenance (Zurli et al., 2025). Devonian strata are generally interpreted as recording sedimentation within a passive margin environment, distant from both the active Devonian volcanic arc and the main paleo-Pacific convergent margin (Glen and Cooper, 2021). By the Permian, sectors of the Transantarctic Basin proximal to the Antarctic Peninsula and the South America sector of Gondwana experienced convergent deformation associated with the Gondwanide Orogen. During this time, these regions also began to receive sedimentary input from a volcanic arc (Elliot, 2013). Consequently, the southern and central portion of the Transantarctic Basin are interpreted as a *retro*-arc foreland basin (Collinson et al., 1994). In contrast, the northern portion of the Transantarctic Basin is regarded as an intracratonic basin, owing to its long distance from the paleo-Pacific margin and the Gondwanide Orogen, its limited thickness, absence of deformation, and dominantly cratonic sediment source. The northern and central sectors were separated from the northern sector by the Ross High (Collinson et al., 1994), which likely acted as a structural divide between the two sub-basins until the Early Triassic: a foreland basin to the south, and a cratonic basin to the north (Fig. 1b). Subsequent burial of the Ross High led to the merging of these sub-basins into a unified basin system (Collinson et al., 1994; Zurli et al., 2024a). The entire sedimentary sequence is characteristically intruded by numerous thick dolerite sills and dike swarms belonging to the Early Jurassic (~180 Ma) Ferrar Large Igneous Province. This magmatism records the rifting and volcanism associated with the onset of Gondwana breakup and the development of the modern southern continents (e.g., Elliot, 1992; Encarnación et al., 1996; Elliot et al., 2021; Elliot and Fleming, 2021).

Significant stratigraphic variation characterizes the Beacon Supergroup across the Transantarctic Mountains (TAM) (Fig. 1b). The contrasting presence of Devonian strata between southern and northern Victoria Land, coupled with the localized absence of lower Permian deposits in specific sub-basins, raises critical questions regarding the role of paleo-topography and the extent of erosional episodes that influenced deposition. Large stratigraphic gaps (unconformities; e.g.,

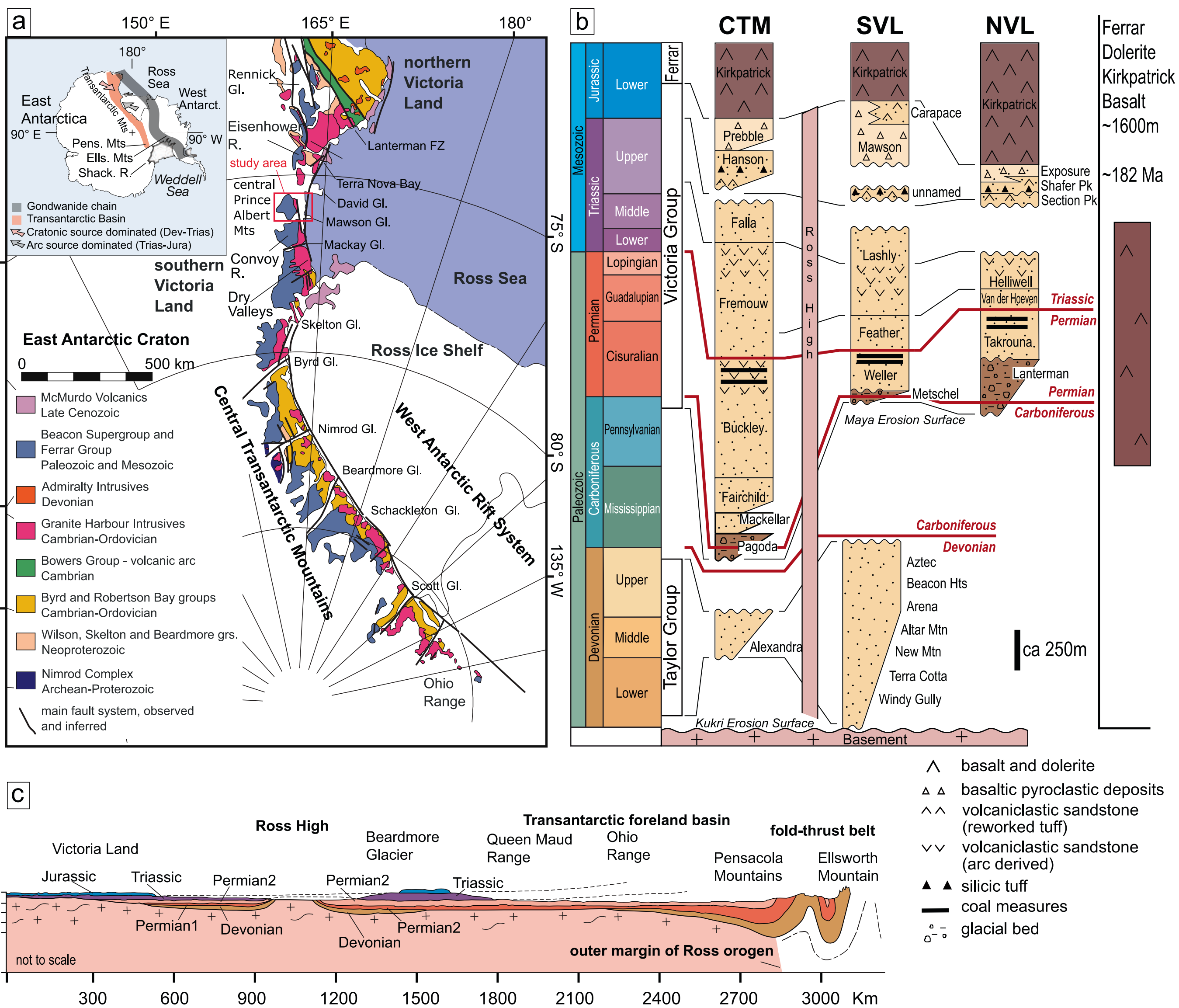

Fig. 1. (a) Geologic and tectonic map of the TAM (modified from Goodge 2020). The insert shows the inferred present remnant location of the Gondwanide Orogen and the provenance of the Beacon Supergroup sediments for the Victoria Land. (b) Simplified stratigraphy of the Beacon Supergroup along the Transantarctic Mountains. The vertical dimension is to scale (modified from Elliot, 2013; Cornamusini et al., 2023 and references therein). Maximum cumulative thickness of Ferrar Dolerite sills is also represented but the stratigraphic position of the sills within the Beacon supergroup and basement is not shown. (c) Schematic composite cross section across the Transantarctic Basin just before the Ferrar volcanic event, redrawn after Collinson et al. (1994).

the Maya Erosion Surface, Harrington, 1965; McKelvey et al., 1977) indicate either prolonged periods of non-deposition (typically associated with topographic highs) or subsequent erosional phases. Identifying, constraining the timing of, and interpreting these erosional phases within the Beacon Supergroup successions can provide critical insights into crustal-scale processes and the resulting *syn*-tectonic depositional environments of the Transantarctic Basin. In this context, the Devonian-Jurassic sedimentary archive of the Transantarctic Basin system offers crucial geological records for reconstructing the long-term environmental and tectonic evolution of the East Antarctica craton through space and time.

This study integrates petrographic and stratigraphic data from the Victoria Group sandstones of the Beacon Supergroup with thermochronological data (apatite fission-track (AFT) and zircon (U-Th)/He (ZHe) dating collected from crystalline basement and Ferrar Dolerites in the Prince Albert Mountains region of southern Victoria Land (Fig. 1a). The primary goal is to refine the Permian–Triassic evolution of the Transantarctic Basin within the broader context of the intracratonic evolution and fragmentation of the Gondwana Supercontinent.

2. Geological setting

The TAM mark the physiographic boundary between East and West Antarctica and preserve a polyphase geological history, spanning the supercontinent cycle since ~ 3.1 Ga (Goodge, 2020). During the Neoproterozoic to early Paleozoic, the TAM portion of East Antarctica evolved from a passive to an active continental margin, becoming part of the Ross-Delamerian orogenic system along the paleo-Pacific margin of Gondwana (e.g. Stump, 1992, 1995; Goodge, 2020). The Ross Orogeny in Antarctica developed as an Andean-type convergent margin, characterized by extensive magmatic arc activity. These magmas intruded Proterozoic to early Paleozoic crust, resulting in the formation of the Granite Harbour Intrusives, dated between 580 and 470 Ma (Goodge, 2020). A prolonged phase of tectonic stability began during the Late Ordovician, resulting in extensive erosion that gradually reduced the Ross Orogenic Belt to a low-relief erosional surface known as the Kukri Erosion Surface (McKelvey et al., 1977). The Kukri Erosion Surface is recognizable throughout the TAM, except in northernmost Victoria Land, approximately north of Lanterman Fault Zone (Fig. 1a; Balestrieri et al., 2020). Overlying the Kukri Erosion Surface, the lithostratigraphy of the Gondwana sequence is dominated by continental-derived siliciclastic deposits of the Beacon Supergroup (Barrett et al., 1971). These deposits crop out from Victoria Land across the TAM to the Pensacola Mountains and Shackleton Range in the Weddel Sea region (Fig. 1a), with thicknesses ranging from tens of meters up to 2500–3000 m along the TAM. The Beacon Supergroup comprises Devonian continental and shallow-marine deposits of the Taylor Group, transitioning across the Maya Erosion Surface to upper Carboniferous to lower Permian glacigenic deposits of the Victoria Group. This succession is overlain by Permian alluvial deposits and coal measures, followed by Triassic alluvial deposits and Lower Jurassic alluvial-volcaniclastic units (Fig. 1b; McKelvey et al., 1970; Barrett et al., 1971; Barrett, 1981, 1991; Collinson et al., 1994; Elliot, 1996, 2013, Di Giulio et al., 1999; Schöner et al., 2007; Bradshaw, 2013; Bomfleur et al., 2021; Cornamusini et al., 2023).

During the Devonian, the Transantarctic Basin was mainly supplied by sediments derived from the erosion of the Ross Orogen and the East Antarctic craton (Barrett, 1991) and it is considered as an epicratonic basin associated with a passive continental margin. In this context, the Devonian Taylor Group, which overlies the Kukri Erosion Surface, shows a thicknesses ranging from few hundreds of meter in central TAM to 1.4 km in southern Victoria Land, while it disappears in northern Victoria Land. This pattern suggests the presence of a topographic high in the northernmost TAM, associated with a Devonian deformational and magmatic event (e.g. Lisker et al., 2006; Glen and Cooper, 2021). Lower Carboniferous rocks are absent throughout the TAM, whereas upper Carboniferous to lower Permian glacigenic strata occur discontinuously and exhibit variable thickness across the region. These deposits rest disconformably on Devonian strata in the central TAM and southern Victoria Land, and on Ross-aged basement in the northern Victoria Land (Fig. 1b) (Veevers, 2004; Isbell et al., 2008; Isbell et al., 2012; Koch and Isbell, 2013; Cornamusini et al., 2017; Zurli et al., 2022). Glacigenic sedimentation in the TAM is interpreted to have initiated in the late Carboniferous and persisted into the earliest Permian (Kyle, 1977; Cornamusini et al., 2017). The maximum thickness, approximately 250 m, is recorded in northern Victoria Land (Lanterman Range, Fig. 1a). Provenance studies indicate a major contribution from the local basement, together with reworked Devonian sandstones (Elliot et al., 2015; Zurli et al., 2022, 2024b). The Permian strata rest disconformably atop the underlying glacigenic deposits across both the central TAM and Victoria Land. These formations are characterized by widespread coal beds, particularly in their upper intervals (Fig. 1b). During the Permian, the southern sector of the Transantarctic Basin is interpreted as a back-arc basin, with sedimentary records reflecting the dismantling of the Gondwanide volcanic arc. In contrast, the northern sector (present-day Victoria Land) is considered an epicratonic/backbulge basin, located distal to the deformational front and receiving sediment input primarily from the crystalline rocks of the Ross Orogen (Collinson et al., 1994; Elliot et al., 2017; Zurli et al., 2024a). In central TAM, Permian strata are dominated by volcanic grains (Barrett et al., 1986), which have been dated to the Permian (Elliot et al., 2015). In contrast, sandstones from southern and northern Victoria Land exhibit a quartz-feldspar-dominated composition (Collinson et al., 1986; Cornamusini et al., 2023; Zurli et al., 2024a). Triassic strata are thicker in the central TAM and southern Victoria Land then in northern Victoria Land, where Lower to Middle Triassic strata are sparse and exposed only in the lower Rennick Glacier area (Bomfleur et al., 2021). In the Deep Freeze Range and upper Rennick Glacier, the Upper Triassic-Jurassic Section Peak Formation rests directly on crystalline basement, whereas in the lower Rennick Glacier it disconformably overlies older Triassic strata (Bomfleur et al., 2021). A consistent feature across all Triassic deposits is the marked increase in volcanic-arc detritus from the late Early to Middle Triassic, indicating a closer proximity of the Transantarctic Basin to the magmatic arc associated with the Gondwanide orogen (Barrett et al., 1986; Collinson et al., 1994; Di Giulio et al., 1999; Elliot et al., 2015, 2017, 2019; Bomfleur et al., 2021; Cornamusini et al., 2023; Zurli et al., 2024a). Between southern Victoria Land and the central TAM, the Ross High (Collinson et al., 1994) formed a persistent topographic basement high from the Devonian to the Triassic. This structure inhibited the deposition of the Beacon Supergroup between the Nimrod and Byrd glaciers. The Ross High is interpreted as a forebulge that separated a foreland basin to the south from an epicratonic/backbulge basin to the north (Collinson et al., 1994).

Deposition of the Gondwana sequence concluded in the Early Jurassic with the emplacement of the Ferrar Large Igneous Province, dated at 182.6 ± 0.2 (zircon U-Pb; Burgess et al., 2015). This event represents fast emplacement of subvolcanic and volcanic products (Ferrar Dolerite and Kirkpatrick Basalts) associated with the initial breakup of the Gondwana supercontinent, which had remained tectonically stable for nearly 300 Myr, between ~ 450 and ~ 180 Ma. The original thickness of the Ferrar Dolerite and Kirkpatrick Basalts remain uncertain due to subsequent erosion and generally poor expositions. The Ferrar Dolerite was emplaced at shallow crustal levels, and multiple lines of evidence indicate that intrusion occurred close to the surface (Prenzel et al., 2014, 2018). Subsequent reheating produced temperature increases of approximately 50–125 °C across several areas of northern Victoria Land. (Molzahn et al., 1999; Lisker, 2002; Bernet and Gaupp, 2005). In the southern Prince Albert Mountains, the present thickness of Ferrar volcanic products is estimated at approximately 1600 m, consistent with the thickness in the Convoy Range to the south (Wörner 1992; Elliot et al., 2021; Capponi et al., 2024).

The emplacement of the Ferrar Supergroup marks the beginning of an extensional regime that, through multiple phases, persisted until the Cenozoic. This prolonged tectonic activity ultimately led to the development of the West Antarctic Rift System, a vast continental extensional domain that separates East Antarctica from West Antarctica. The timing, rate and magnitude of extension remain poorly constrained (Fioraso et al., 2024; Civile et al., 2025) due to the absence of drilled and dated rift-related sediments. A Cretaceous extensional phase is recorded within the basement of the West Antarctic Rift System and across West Antarctica (Siddoway et al., 2004), with only limited evidence along the TAM (Fitzgerald, 2002). This phase produced several hundred kilometers of lithospheric extension and occurred contemporaneously with separation of Antarctica from Australia (Siddoway, 2008; Jordan et al., 2020). Thermochronological modeling from northern Victoria Land, particularly inland of the Terra Nova Bay, supports the existence of a large sedimentary basin, the Mesozoic Victoria Basin, active from the Middle Jurassic to the late Eocene (Lisker and Läufer, 2013; Prenzel et al., 2013, 2014, 2018).

The most well-documented phase of rifting spans from the middle Cenozoic to the present and is associated with the major uplift and exhumation that shaped the steep front of the TAM. Low-temperature thermochronological data indicate that erosion intensified along the TAM front during the Eocene–Oligocene (~45–33 Ma) (Fitzgerald, 1992; Rossetti et al., 2003; Fitzgerald et al., 2006; Miller et al., 2010; Prenzel et al., 2018; He et al., 2021). This exhumation resulted from rift-shoulder uplift, further enhanced by transtensional shearing (Rossetti et al., 2006; Storti et al., 2007; Vignaroli et al., 2015; Fioraso et al., 2025). Cenozoic tectonics strongly influenced the topography of the eastern TAM front, producing a steep escarpment (e.g. Behrendt and Cooper, 1991; Fitzgerald, 1992; Sugden et al., 1995; Sugden and Denton, 2004; Olivetti et al., 2018). The onset of Antarctic glaciation may have further accelerated erosion during the Eocene–Oligocene transition (He et al., 2021; Prenzel et al., 2014). Thermochronological data indicate that erosion along the TAM front removed several kilometers of rock (Fitzgerald, 2002; Prenzel et al., 2014; He et al., 2021; Miller et al., 2010; Balestrieri et al., 2020).

The study area encompasses the central sector of the Prince Albert Mountains, extending from the Royal Society Range in the south to the Eisenhower Range in the north (Fig. 1). In this region, Beacon Supergroup deposits unconformably overlie the Late Proterozoic-Early Palaeozoic continental basement, composed of metaluminous and peraluminous granitoids belonging to the Granite Harbour Intrusives (Gunn and Warren, 1962; Stump, 1995; Rocchi et al., 1998; Goodge, 2002). Outcrops of the Beacon Supergroup in this sector of the TAM are limited in extent and stratigraphic continuity, often occurring as isolated bodies within the Jurassic Ferrar Dolerite. The timing of deposition is poorly constrained. The geological map reports only one locality, Beta Peak, where *Glossopteris flora* has been identified, indicating the presence of Permian strata (Capponi et al., 1999). Fossil evidence from Benson Knob in the southern Ricker Hills (Fig. 2) provides further age constraints. Compressions of *Dicroidium* leaves and fossil wood are assigned to the Triassic Section Peak Formation (Capponi et al., 1999; Oh et al., 2019). Moreover, an Early Jurassic palynofloral assemblage has been documented at McLea Nunatak (Fig. 2a; Unverfärth et al., 2020). At Mount Smith, a few meters of Beacon sandstone overlie the Granite Harbour Intrusives along the eastern cliff, exposing the contact with the basement (Capponi et al., 2020). Upper Carboniferous-lower Permian glacigenic deposits are absent throughout the study area, but they occur both to the north in the Eisenhower Range and to the south in northern Convoy Range (Elkhorn Ridge) (Fig. 1a, Fig. 2a).

3. Methods and sampling

3.1. Field work and sandstone petrography

Field investigations in the central Prince Albert Mountains were carried out during the XXVIII (2012–2013), XXXI (2015–2016), XXXIII (2017–2018) and XXXIV (2018–2019) Italian National Antarctic Research Program (PNRA) expeditions. Thermochronological sampling was performed along two transects oriented orthogonally to the TAM front, extending from the coastal margin to the most interior outcrops. The northern transect follows approximately the 75°45′ S latitude (Fig. 2a), whereas the southern one is aligned with the 76°10′ S and it includes a vertical profile along the eastern flank of Mount Murray (Fig. 3a). A total of 12 samples were collected: four from the northern transect and eight from the southern one, respectively. Apatite grains from all samples were analyzed using the fission-track method, while zircon grains from five representative samples, selected based on elevation, distance from the coast, and lithology, were dated using the (U-Th)/He method. A further 37 samples of the Beacon Supergroup sandstones were collected for petrographic analysis from five outcrops distributed from south to north: The Mitten, Pudding Butte, Ricker Hills-Benson Knob, Ford Peak and Trio Nunatak, respectively. Compositional petrographic analyses were conducted using the Gazzi-Dickinson point counting method (Gazzi, 1966; Ingersoll et al., 1984). All collected samples are curated at the Italian National Museum of Antarctica, Siena section.

3.2. Thermochronological analysis

Apatite and zircon grains were separated from the 100–160 μm fraction of approximately 3 kg of crushed-rock samples, using standard magnetic and heavy-liquid procedures at the Department of Geosciences laboratory, Padova University. For apatite fission-track analysis, grains were mounted, grounded, polished, and etched with 5 % HNO_3 at 20 °C for 20 s to reveal the spontaneous tracks. The mounts were prepared in external detector configuration using low-U muscovite sheet then irradiated with thermal neutrons in the Radiation Center of the Oregon State University. After the irradiation, the muscovite detectors were etched in 40 % HF at 20 °C for 40 min to reveal the induced fission tracks. The AFT ages were calculated using the external detector and ζ-calibration methods, with a ζ-value of 355.02 ± 4.36 for dosimeter CN5, calibrated against Fish Canyon Tuff and Durango apatite standards (Hurford, 1990; Hurford and Green, 1983).

The (U-Th)/He analyses were performed at the Low-Temperature Thermochronology Laboratory of the Institute of Rock Structure and Mechanics of the Czech Academy of Sciences. Fish Canyon Tuff zircon was used to assess analytical uncertainties. Zircon grains were loaded into niobium (Nb) tubes and heated to 900–1200 °C using a high-energy diode laser beam. Released ^{4}He was measured with the integrated Pfeiffer quadrupole mass spectrometer of the automated Alphachron system. Degassed grains were then dissolved in concentrated HNO_3 and HF and spiked with standards containing known U and Th concentrations. The amounts of ^{238}U, ^{235}U, ^{232}Th, and ^{147}Sm were measured using a ThermoFisher Scientific ELEMENT 2 ICP-MS at the Institute of Geology of the Czech Academy of Sciences.

3.3. Zircon (U-Th)/He thermochronology and date-eU correlation

Zircon (U–Th)/He (ZHe) dating is a routinely used thermochronological technique with an experimental closure temperature of about 180 °C (Reiners et al., 2002). However, natural samples can show a much broader closure-temperature range, from values of about 200 °C to temperature lower than those of the AFT system (Wolfe and Stockli, 2010; Guenthner et al., 2017; Gérard et al., 2022). This variability is largely attributed to the high level of radiation damage, which increases the He diffusivity and may result in anomalously young ages (Guenthner et al., 2013, 2014). Zircon typically contains high concentrations of U and Th, quantified as effective uranium (eU). As damage accumulates, eU can exceed the threshold of interconnected damage zones (α-dose > 1.5×10^{18} α/g), leading to the development of fast-diffusion pathways (Guenthner et al., 2013). In many datasets, this process produces a negative correlation between ZHe ages and eU (Guenthner et al., 2017).

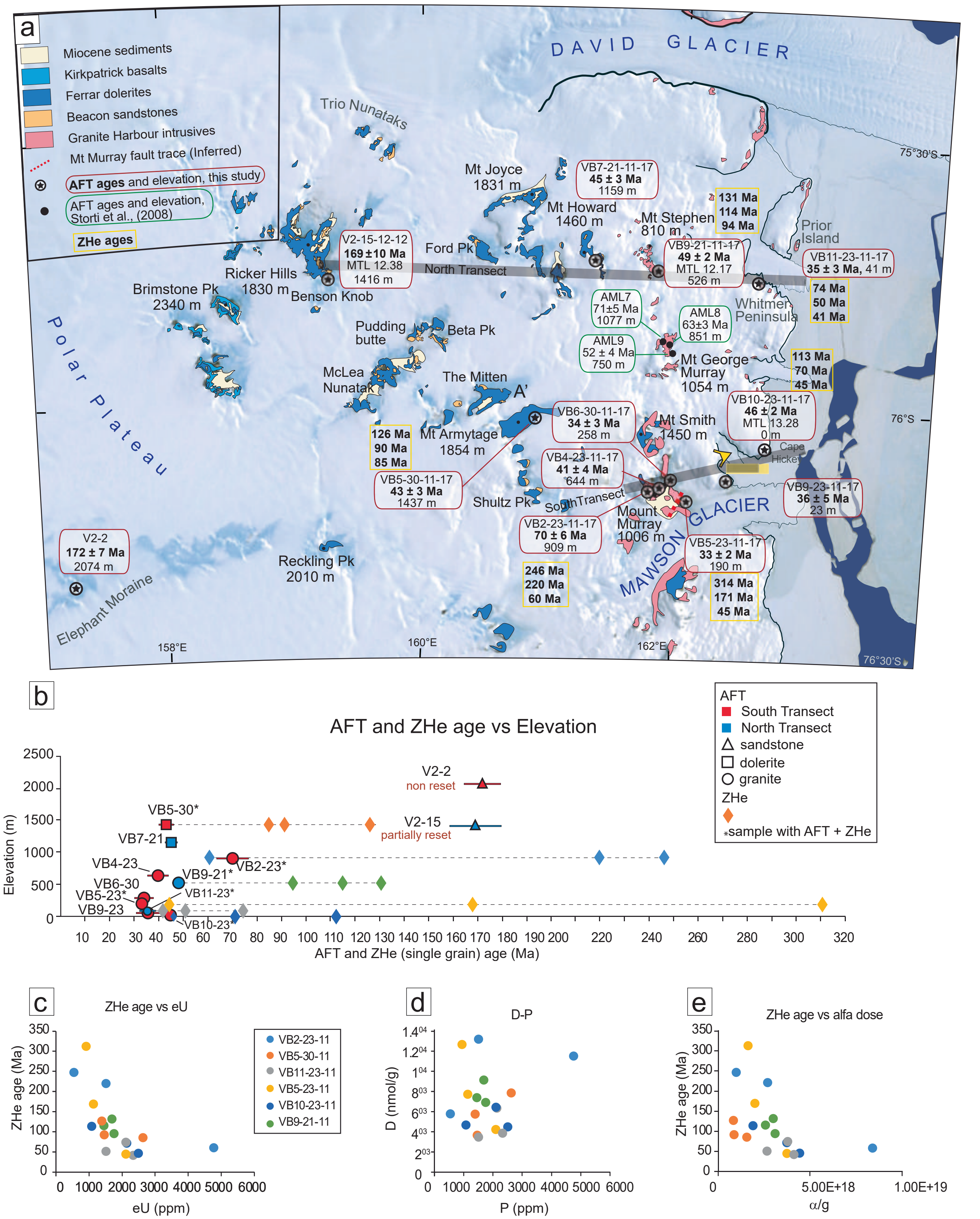

Fig. 2. (a) Satellite image of the central Prince Albert Mountains (study area) with the lithology, sampling sites and thermochronological data (lithology is based on Capponi et al., 1999; Capponi et al., 2020). (b) Age-elevation relationship of the AFT ages and ZHe (single grain) ages. (c) Content of the eU vs single ZHe grain age. (d) Daughter-parent (D-P) plot for each sample. (e) Radiation damage alpha-dose vs single ZHe grain age.

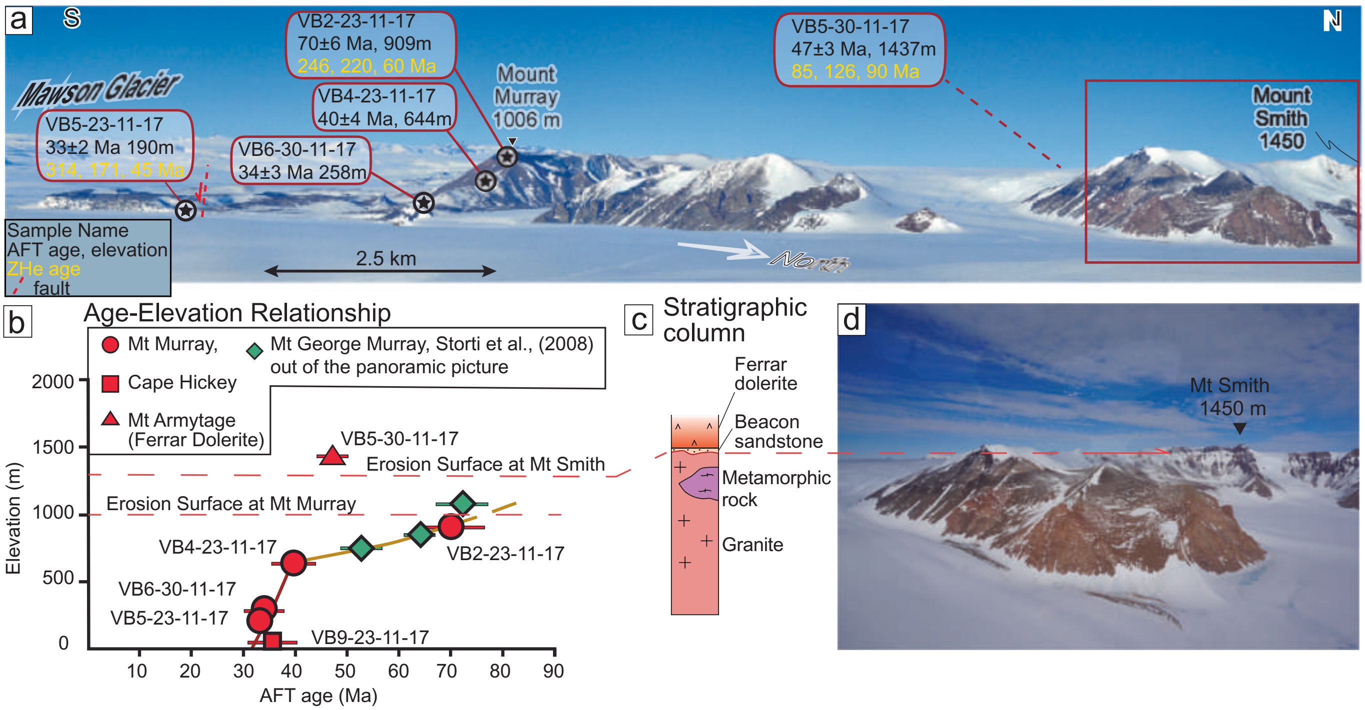

Fig. 3. (a) Aerial photo of the eastern flank of Mount Murray and Mount Smith (see Fig. 2 for location). Photo shows the thermochronological data and location of Mount Murray samples used for modeling. Sample of dolerite is located background, back to Mount Smith. Tectonic structure between sample VB5-23–11-17 and Mount Murray vertical profile is shown. (b) AFT age-elevation relationship for the samples from Mount Murray (this study) and from Mount George Murray (Storti et al., 2008). Samples from Mount Murray and Mount George Murray show two rectilinear trends joint in a break in slope testifying two periods of constant but different exhumation rates, an older and slower and a younger and faster. Mount Armytage sample is out of the trend and higher than sample from Mount Murray with the same age. The red line marks the location of the Kukri Erosion Surface. (c) Sketch of the stratigraphic column of Mount Murray and Mount Smith representing the elevation of the Kukri Erosion Surface on top of the crystalline basement and the thickness of the Beacon sandstone. (d) Aerial photo of Mount Smith showing the crystalline basement made of Granite Harbour Intrusives Complex and darker metamorphic rocks, the Kukri Erosion Surface that underlain the thin Beacon sandstone and the Ferrar Dolerite on top. (For interpretation of the references to colour in this figure legend, the reader is referred to the web version of this article.)

However, such correlations can also be spurious and may yield misleading thermal histories (Härtel et al., 2022). Distinguishing causal from non-causal relationships ideally requires independent damage measurements or large datasets allowing robust dispersion–predicted (D–P) plot analyses (Härtel and Enkelmann, 2024), although these conditions are not always attainable. When direct measurements are unavailable, evaluating radiation-damage levels using uranium content, crystallization age, α-dose–age trends, and the consistency among modeled thermal histories can help clarify the role of damage on the He retention. In such cases, applying the zircon radiation-damage accumulation and annealing model (ZRDAAM) of Guenthner et al. (2013) provides a framework to interpret large age dispersion and to recover reliable long-term thermal histories from multigrain ZHe datasets.

4. Results

4.1. Beacon Supergroup stratigraphy and composition

The Beacon Supergroup was examined at five outcrops within the study area, yielding 37 sandstone samples from different stratigraphic levels (Fig. 2a). Samples were classified using a ternary diagram based on the relative proportion of quartz, feldspar and rock fragments (Fig. 4). At Ford Peak, the stratigraphic section is approximately 20 m thick and consists of fine- to very coarse-grained sandstones, locally pebbly and commonly exhibiting trough cross-bedding. Thin mudstone interbeds, locally carbonaceous, are present. The seven sandstone samples are dominated by mono- and polycrystalline quartz, with minor alkali feldspars, plagioclase, and metamorphic lithic fragments. White mica and biotite are present in some layers. The Pudding Butte section, ~50 m thick, is composed of medium- to very coarse-grained sandstones, locally pebbly, with trough cross-bedding. Bioturbation and reddish encrusted layers are widespread. The eight samples contain abundant monocrystalline quartz, whereas feldspar and metamorphic lithic fragments are rare. At the Mitten, the outcrop comprises ~ 25 m of alternating medium to coarse-grained trough cross bedded sandstones and mudstones, with occasional carbonaceous layers. The section at Trio Nunatak is discontinuous due to snow and debris cover but includes medium- to very coarse-grained and locally pebbly trough cross bedded sandstones interlayered with mudstones. Bioturbation and soft sediment deformation structures occur in the lower section, while fossil wood fragments characterize the upper levels. Most samples from Ricker Hill come from a section correlatable with that described by Oh et al. (2019), consisting of medium- to coarse-grained trough cross-bedded sandstones with Triassic fossil woods in the uppermost strata. Sample V2-15–12-12 was collected from an overlaying layer at Benson Knob, near mudstone containing *Dicroidium* leaf impressions, as also reported by Capponi et al. (1999). Sample C10-15–12-12 derives from the uppermost part of the Benson Knob section, where siliciclastic strata alternate with felsic tuffaceous layers. Samples from The Mitten, Trio Nunatak, and Ricker Hills show similar mineralogical composition (Fig. 4), mainly consisting of monocrystalline quartz and altered fine-grained mafic to felsic volcanic lithic fragments, with minor metamorphic lithics and alkali feldspars. The uppermost stratigraphic sample (C10-15–12-12) lacks lithic fragments.

4.2. Apatite fission-track and ZHe data

Most samples (nine out of twelve) were collected from the Granite

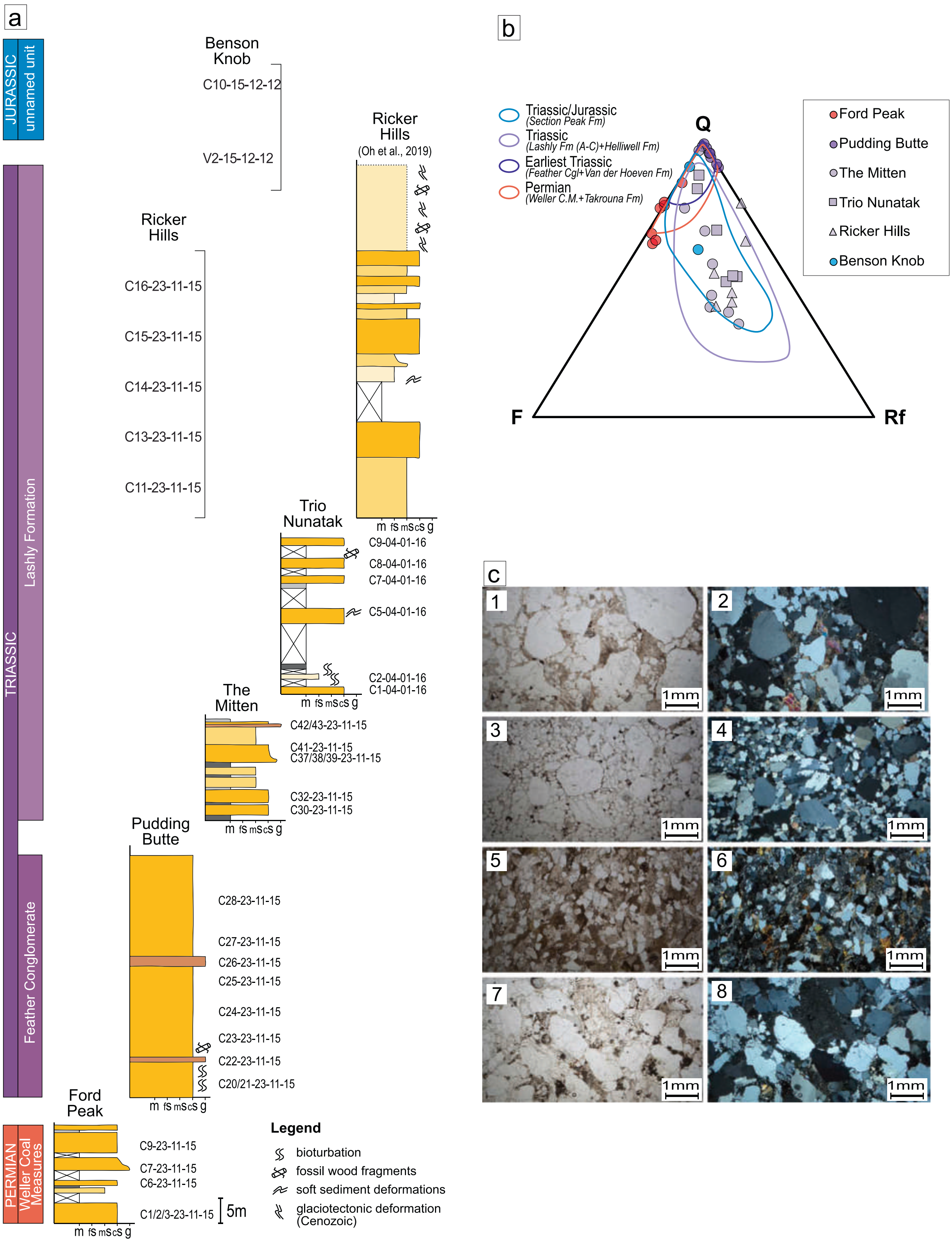

Fig. 4. Stratigraphic logs of the studied Beacon Supergroup successions in the central Prince Albert Mountains; the position of the samples analyzed for quantitative petrography is shown. The log of Ricker Hills is modified from Oh et al. (2019). m: mudstone, fS: fine sandstone, mS: medium sandstone, cS: coarse sandstone, g: gravel; (b) Quartz-Feldspar-Rock fragments (Q-F-Rf) ternary diagram showing the composition of the Beacon Supergroup sandstones from the studied outcrops. Compositional fields are based on Korsch (1974), Walker (1980), Collinson et al. (1983, 1986), Di Giulio et al. (1999), Bernet and Gaupp (2005), Cornamusini et al. (2017, 2023), Zurli et al. (2024a); (c) Microphotographs representative of the Beacon Supergroup sandstones from central Prince Albert Mountains: (1–2) C6-23–11-15; (3–4) C21-23–11-15; (5–6) C16-23–11-15; (7–8) C10-15–12-12.

Harbour Intrusives, composed of unfoliated to weakly foliated metaluminous biotite granites. The remaining samples include one from the Ferrar Dolerite at Mount Armytage, one Beacon sandstone from the Section Peak Formation at Richer Hills, and one loose detritus sample from Elephant Moraine, a marginal moraines of the polar plateau to the east. AFT ages range from 180 ± 11 Ma to 33 ± 2 Ma and generally correlate with elevation (Fig. 2). Only three samples (VB9-21–11, VB10-23–11, V2-15–12) contained enough confined tracks to measure mean track lengths (MTL), which vary between 12.38 μm and 13.38 μm. Complete fission-track data are shown in Table S1.

The ZHe dating was performed on 18 grains from six samples (five from the Granite Harbour Intrusives and one from the Ferrar Dolerite) (Fig. 2a; Table S2). The ZHe ages span from 311 Ma to 41 Ma and exhibit considerable internal variability, including several ages younger than the corresponding AFT ages. The eU content varies widely among aliquots, from 554 ppm to 4772 ppm, with only two aliquots below 1000 ppm. Ages are negatively correlated with the eU (Fig. 2c), reflecting the well-known effect of radiation damage on He retention in high-eU zircon (Guenthner et al., 2013). Daughter-parent (D-P) plots show poor correlation due to the limited number of aliquots (Fig. 2d). However, alphadose vs age relationships are negatively correlated, suggesting that differences in single-grain ages are primarily controlled by radiation-damage accumulation (Fig. 2e). The thermochronological data are described along two sampling transects, southern and northern, oriented from west to east (Fig. 2a).

4.2.1. Southern transect and Elephant Moraine

The southern transect includes six samples collected along a profile extending from the coastal area at Cape Hickey to the summit of Mount Murray. Furthermore, the study incorporated one sample from the Ferrar Dolerite (located just outside the transect trace) and one from Elephant Moraine (approximately 120 km to the east). Elephant Moraine lies at the edge of the Polar Plateau and consists of unconsolidated, poorly sorted moraine detritus transported by active glacial processes. Sample V2-2, composed of ∼ 2 kg of medium sand, passed the χ^2 test for AFT age distribution, suggesting a single population. The resulting AFT age is 172 ± 7 Ma, consistent with the volcanic event of the Ferrar Supergroup (∼182 Ma; Elliot et al., 2021).

Mount Armytage – A medium-grained dolerite (microgabbro, sample VB5-30–11-17) was collected to obtain apatite and zircon grains suitable for thermochronology. This sample provides one of the few thermochronological ages from Ferrar Dolerite along the entire TAM. The AFT age is 47 ± 3 Ma, while three ZHe ages are 126, 90, and 85 Ma, respectively, with corresponding eU contents of 1398, 1466, and 2637 ppm. ZHe ages show a negative correlation with eU, consistent with radiation-damage-controlled He retention.

Mount Murray profile – Three samples (VB2-23–11-17; VB4-23–11-17; VB6-30–11-17) were collected along a near-vertical profile from 258 m asl at the base of the cliff to 909 m asl, a few tens of meters below a Ferrar Dolerite sill. In this portion of the TAM, Capponi et al. (2020) observed that the lowermost Ferrar sill generally rests directly on the Kukri Erosion Surface, with no intervening Beacon sandstones. However, thin, meter-thick bodies of Beacon sandstones have been occasionally observed interlayered between the Ross basement and the Ferrar Dolerites (e.g., at Mount Smith). The AFT age-elevation diagram for Mount Murray shows a break in slope, with the uppermost sample residing longer within the Partial Annealing Zone than the lower two. The AFT ages correlate with the elevation, ranging from 70 ± 6 Ma at the top (VB2-23–11-17), to 40 ± 4 Ma for the intermediate sample (VB4-23–11-17) and 34 ± 3 Ma for the lowermost sample (VB6-30–11-17). Zircon grains from the uppermost sample (VB2-23–11) yielded ZHe ages of 246, 220, and 60 Ma, negatively correlated with eU values of 554, 1522, and 4772 ppm, respectively. The age-elevation relationship mirrors other Victoria Land profiles in terms of the break in slope and the slope of the segments above and below the break (Fitzgerald, 1992; Prenzel et al., 2014, 2018).

Lower Mount Murray area – Sample VB5-23–11-17, located ∼ 4 km from the base of the vertical profile at 190 m asl, shows an AFT age of 33 ± 2 Ma. Three zircon grains yielded ZHe ages of 314 Ma, 171 Ma and 45 Ma, reflecting differences in eU content (918, 1136, 2115 ppm). This sample was analyzed separately due to a major tectonic structure encountered in the field, consisting of a complex N–S-striking fault zone with normal to oblique-normal kinematics (Fig. S1). Although the AFT age is comparable to other low-elevation samples (VB11-23–11-17, VB10-23–11-17), the ZHe results include two older ages, which will be discussed in more detail in sections 6.4.

Cape Hickey – Sample VB9-23–11-17, collected at 23 m asl, yields an AFT of 36 ± 5 Ma. Another sample at sea level (VB10-23–11-17) gives an AFT age of 46 ± 2 Ma with a MTL of 13.28 μm (60 track, not projected). Zircon analyses from this sample produced three corrected ZHe ages of 113, 70, and 45 Ma, which correlate with the eU values of 1084, 2107, and 2513 ppm, respectively.

4.2.2. Northern transect

Benson Knob – Sample V2-15–12 was collected from Beacon sandstone at Ricker Hills (Fig. 2A), at 1416 m asl. It is among the westernmost samples analyzed along the TAM and the closest to the Polar Plateau. The Beacon strata in this area are tilted and plunge slightly westward toward the Polar Plateau. Therefore this sample represents the uppermost stratigraphic levels. It belongs to the inferred Triassic-lowestmost Jurassic part of the Beacon succession. A total of 50 apatite grains were separated, yielding a central AFT age of 169 ± 9 Ma. Thirty track lengths were measured, giving a MTL of 12.38 μm. Grain-age dispersion is high, and the sample fails the χ^2 test. The deconvolution into populations of age reveals an older than stratigraphic age population (297 ± 53 Ma), a second population of 195 ± 43 Ma that matches the age of the Ferrar Dolerite (∼182 Ma, Elliot et al., 2021) and the most abundant population that is younger than Ferrar Dolerite (Table S1). These features suggest partial resetting of the sample due to post-sedimentation heating, followed by slow cooling.

Mount Howard – A Ferrar Dolerite sample (VB7-21–11-17) was collected at 1159 m asl, yielding an AFT age of 45 ± 3 Ma. This is consistent with other dolerite samples from Mount Armytage. Given the shallow emplacement of the dolerite, this AFT age likely reflects a reheating event followed by Eocene cooling, similar to basement samples.

Mount Stephen – A Granite Harbour Intrusive sample (VB9-21–11-17) was collected at 526 m asl along the flank of Mount Stephen. The AFT age is 48 ± 2 Ma, with a MTL of 12.17 μm (not projected, 48 track lengths). Three zircons from this sample yielded ZHe ages of 131, 114, and 94 Ma, respectively. The oldest grain shows no clear correlation between the eU content and the ZHe age.

Whitmer Peninsula – A sample of Granite Harbour Intrusive complex (VB11-23–11-17) was collected along the northern coast of the Whitmer Peninsula at 41 m asl. The AFT age is 35 ± 3 Ma. Three zircon grains yielded ZHe ages of 74, 50 and 41 Ma, respectively. The ages appear negatively correlated with the eU content (1504, 2337 and 2120 ppm respectively). The oldest grain is notable for its high eU concentration, despite its age.

5. Temperature-time modeling

The thermal history modeling aimed to identify the temperature–time (T-t) paths that optimally reproduce the observed zircon age-eU correlations and the AFT data. Crucially, these paths must also remain consistent with stratigraphic constraints and all published thermochronological and geological data. We used QTQt software (Gallagher, 2012), in both inverse and forward modes, applying the ZRDAAM of Guenthner et al. (2013) to explore a wide temperature range driven by the strong eU variability. Although a spurious age-eU cannot be entirely ruled out, the high radiation damage level and the observed correlations support the reliability of ZRDAAM-based modeling.

Models were run in a T-t space spanning 500 Ma to present and 300° C to 0 °C, with the following prior constraints: (i) Cambrian magmatic and subsequent exhumation of the Ross-age basement; (ii) near-surface conditions during Beacon Supergroup deposition, varying according to the estimated distance from the Kukri Erosion Surface; and (iii) post-Beacon reheating associated either with Ferrar Dolerite emplacement (temperature peak at 180 Ma) or with burial beneath Mesozoic strata of the Victoria Land Basin (temperature peak during the Mesozoic–early Cenozoic). For the Ferrar Dolerite sample VB5-30–11-17, modeling started from Early Jurassic crystallization followed by a rapid volcanic cooling. Several samples were modeled, under both scenarios (thick Ferrar volcanic cover or burial in a Mesozoic basin). No constraints were imposed for Cenozoic cooling, allowing the inversion to freely estimate timing and rate of final exhumation. During inverse modeling, the paleo–geothermal gradient was left free to vary because QTQt does not permit predefined gradient values as priors.

5.1. Southern transect

Ferrar Dolerite at Mount Armytage – The thermal history modeling of sample VB5-30–11-17 provides unique insights into burial and exhumation of Ferrar Supergroup rocks along the TAM. The model is constrained by AFT ages (no track-length) and ZHe ages, although the two oldest ZHe ages cannot be reproduced simultaneously by applying the ZRDAAM of Guenthner et al. (2013). We initially used forward modeling approach to identify the T-t paths that better replicate the observed data (blue lines in Fig. 5a). Modeling results suggest that, following emplacement, the sample experienced elevated temperatures (up to ~ 200 °C) while three families of thermal histories can fit the dataset (Fig. 5a): (i) rapid post-emplacement cooling followed by immediate reheating and prolonged slow cooling (orange line); (ii) sustained residence at ~ 180 °C and subsequent slow cooling (blue line); (iii) rapid volcanic cooling followed by gradual reheating to a peak temperature of ~ 160 °C between 70–50 Ma, and then rapid cooling (dashed blue line). Inverse modeling with minimal constraints (Fig. 5b, the initial high temperature as the only constrain) produces a Mesozoic reheating phase consistent with the Victoria Basin scenario. Reproducing the Ferrar scenario requires an additional constraint of 120–220 °C between 175–130 Ma. Both reconstructions satisfactorily fit the observed thermochronological data.

Mount Murray profile – The modeling of the Mount Murray profile (Fig. 5c) incorporates three AFT ages from samples collected at 909, 644 and 258 m asl, respectively, and three ZHe ages from the highest-elevation sample. Geological mapping (Capponi et al., 2020) indicates that the highest sample lies ~ 100–300 m below the Kukri Erosion Surface, which in this area is located at an altitude between 1000 and 1300 m asl (Fig. 2). The modeled thermal histories consistently show basement cooling beginning in the Carboniferous–Early Permian and ending during the Permian–Triassic, regardless of the selected thermal scenario (Fig. 5b). Numerous T–t paths remain at low temperatures until the Early Jurassic, implying near-surface exposure before the Ferrar magmatism. During post-Triassic evolution, both thermal scenarios reproduce the observed AFT and ZHe ages, with the Ferrar scenario requiring higher peak temperatures. Although ZHe modeling based on variable eU may be influenced by spurious age–eU relationships (Härtel et al., 2022; Härtel & Enkelmann, 2024), several factors collectively support the robustness of our interpretations:(i) high estimated α-dose levels, (ii) the complexity of the thermal history, implying long residence in the partial retention zone, and (iii) consistent thermal histories across multiple samples, suggesting that eU is the primary driver of intra-sample age dispersion.

Lower Mount Murray area – Sample VB5-23–11-17 (one AFT age and three ZHe ages) was modeled separately because it lies within a complex N–S–striking normal to oblique-normal fault system. The structural context suggests that the sample was downfaulted and therefore originally closer to the Kukri Erosion Surface than its present elevation implies, which is consistent with the two older ZHe ages. To account for this setting, we allowed a broad temperature range during Beacon deposition and tested both post-Beacon thermal scenarios (Fig. 5c). Inverse modeling provides limited constraints on Paleozoic cooling, whereas forward modeling yields a better-fitting T–t path when the Paleozoic cooling window is restricted to the Late Carboniferous–Permian (blue curves in Fig. 5c). Post-Beacon modeling indicates reheating up to ~ 150 °C, and both scenarios satisfactorily reproduce the observed ages and the ZHe age dispersion.

Cape Hickey – Thermal history modeling of sample VB10-23–11-17 is based on three ZHe ages, an AFT age and measured MTL (Fig. 2S) Because the sample sits at sea level and its vertical distance to the Kukri Erosion Surface cannot be determined, we imposed broad Paleozoic constraints and tested both post-Beacon thermal scenarios. Inverse modeling yields a poorly resolved Paleozoic history due to the young ZHe ages, but both thermal scenarios satisfy the observed data (Fig. S2). Forward modeling identifies a preferred T–t path characterized by cooling to near-surface temperatures between the Early Permian and Early Jurassic, similar to results for sample VB5-23–11.

5.2. Northern transect

Beacon sample – Sample V2-15–12-12 shows a large dispersion in grain-age distribution and fails the χ^2 test (Fig. 6a)- Modeling was performed using AFT ages and track lengths, with prior constraints including: (i) a broad crystallization interval, as the apatite source is unknown; (ii) the Triassic–Jurassic depositional age; and (iii) the two alternative post-Beacon scenarios (Fig. 6a; Fig. S3a). Both scenarios reproduce the AFT ages and MTL, although the thick Ferrar volcanic-cover scenario better fits the central age and the oldest grain. The T-t paths before the Early Jurassic remain weakly constrained, while maximum post-Beacon temperature does not exceed 100 °C in both scenarios. We note that modeled T-t histories before 250 Ma represent the thermal evolution of the source region of the apatite grains, as this sample was likely deposited between ~ 250 and 190 Ma. The inferred thermal history is consistent with a Mount Murray–type provenance exhumed around 300 Ma.

Mount Stephen – For sample VB9-21–11-17, collected from the Granite Harbour Intrusives at an altitude of 526 m asl, the absence of an immediately overlying Beacon or Ferrar section prevents the direct application of stratigraphic distances as robust constraints in the analysis. The original position relative to the Kukri Erosion Surface was estimated by noting that at Mount George Murray, a nearby site, Granite Harbour rocks are exposed at 1080 m asl, but without the expected overlying Beacon or Ferrar section. We therefore infer that the local erosional surface at Mount Stephen was at least ~ 1080 m asl, placing sample VB9-21–11-17 at least 600 m below the surface at the time of emplacement of the Ferrar Supergroup. The two thermal history scenarios provide a good fit for the observed thermochronological data, reproducing the two youngest ZHe ages, the AFT ages, and the Mean Track Lengths (MTL) (Fig. 6b, Fig. S3b,c). Neither of the proposed thermal history scenarios successfully reproduces the oldest ZHe ages. We included both the youngest and oldest ZHe ages in the thermal modeling, even though they share similar ages but exhibit contrasting eU values. This approach was adopted because the T–t paths generated are robust; the exclusion of the oldest, potentially inconsistent, grain has a negligible impact on the final thermal solution. Thermal history yields no robust constraints on Paleozoic exhumation, as post-Beacon reheating was high enough to reset pre-existing ZHe ages and erase all Paleozoic thermal history information. This evidence is supported by tests with multiple Paleozoic constraints, all of which produced identical predicted ages. In contrast, the ZHe data constrain maximum reheating, likely because reheating did not exceed ~ 250 °C and was followed by slow cooling, thereby allowing eU-dependent age dispersion to fully develop. Modeling indicates maximum temperatures of ~ 220 °C, ~20

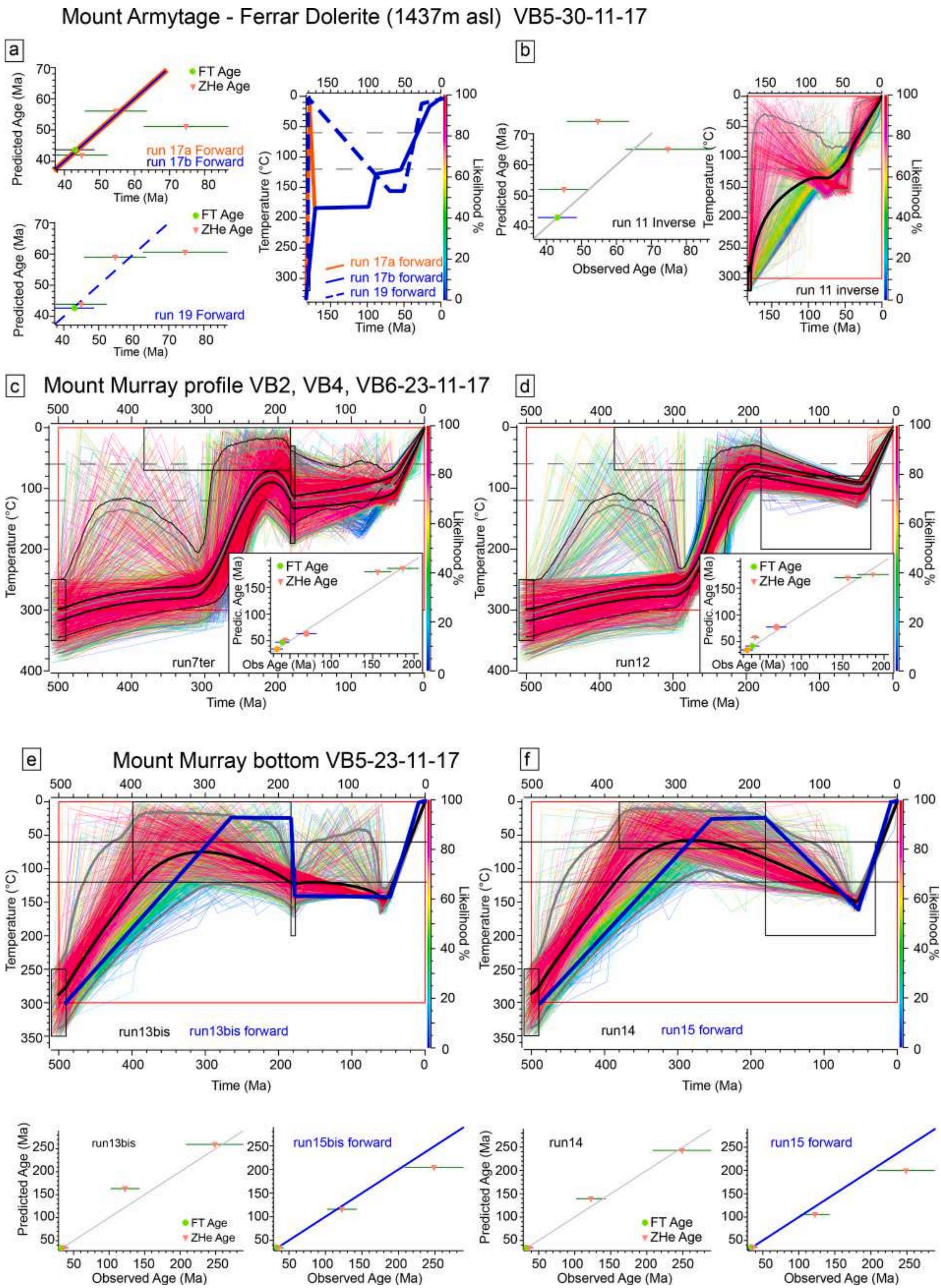

(caption on next page)

Fig. 5. Thermal history modeling results obtained from inverse and forward modeling of combined data (AFT + ZHe) using QTQt software (Gallagher, 2012) by applying FT annealing model of Ketcham et al. (2007) and the ZRDAAM for ZHe data (Guenthner et al. 2013). In the colored inverse modeling plot, the black curves are the expected models and color represents the path probability, and the black boxes represent the Temperature-time constrains. In the Predicted vs Observed ages diagram, the oblique line represents the perfect match between predicted data from the modeling and the experimental data to measure the quality of modeling. (a) Thermal-history paths from forward modeling of the Ferrar Dolerite sample of Mount Armytage (VB5-30–11-17) based on one AFT age and three single grain ZHe ages showing three possible T-t histories, two for the Ferrar scenario (orange and blue lines) and one for the Mesozoic Victoria Basin scenario (dashed blue line). On the left we show the relationship between modeled Predicted and Observed ages for the forward modeling. (b) T-t paths from inverse modeling plotted ranked in order of likelihood probability using the only prior constraint of the dolerite emplacement age. On the left, the relationship between Predicted and Observed ages for the inverse modeling. (c) Thermal-history paths from inverse modeling of the Mount Murray profile (VB2-, VB4-, VB6-23–11-17) based on three AFT ages + three single grain ZHe ages with the modeling constrains for the Ferrar scenario. The insert shows the Predicted vs Observed ages. (d) Same than (c) but with the modeling constrains for the Mesozoic Victoria Basin scenario. The insert shows the Predicted vs Observed ages. (e) Thermal-history paths from inverse modeling and forward modeling (blue line) of the sample at the bottom of Mount Murray. Thermal modeling is based on one AFT age and three single grain ZHe ages with modeling constrain of the Ferrar scenario. In the two panel below, the Predicted vs Observed ages for inverse and forward (blue) modeling are shown. (f) same than (e) but with modeling constrains for the Mesozoic Victoria Basin scenario. (For interpretation of the references to colour in this figure legend, the reader is referred to the web version of this article.)

Myr after the Ferrar event, followed by slow cooling consistent with short MTL values.

Mount Stephen-Whitmer Peninsula –Mount George Murray composite profile – This composite profile (Fig. 6c) integrates five of Ross-aged samples that are not aligned along a single vertical profile but distributed across ~ 25 km. Two samples (VB9-21–11 and VB11-23–11; Fig. 2a), were obtained in this study at 526 m and 41 m asl, respectively, while samples AML7, AML8, and AML9 derive from the Mount George Murray vertical profile (Storti et al., 2008; Prenzel et al., 2018). Modeling incorporates five AFT ages, four track-length datasets, and six ZHe ages. The objective is to test whether these samples share a coherent thermal history and to compare their evolution with the Mount Murray profile. The predicted ages match the observed dataset well, indicating a consistent regional thermal history and limited vertical displacement after Cenozoic cooling. Prior constraints were similar to those adopted for the Mount Murray profile, but with a broader temperature range for the Beacon depositional interval. Modeled T-t paths suggest a maximum post-Beacon temperature of ~ 200 °C, followed by prolonged cooling interrupted by two accelerations: an Early Cretaceous phase (80–100 Ma) and a late Eocene phase (~38 Ma). This thermal evolution agrees with existing reconstructions of the TAM erosion history and better constrains the timing and magnitude of post-Beacon reheating and subsequent exhumation.

6. Discussion

6.1. Stratigraphic correlations

The stratigraphy of the Gondwanan sequences in the central Prince Albert Mountains was reconstructed through field observations and sandstone compositional analyses and correlated with adjacent sectors of the Transantarctic Basin. The oldest Beacon Supergroup strata in the study area are of Permian age, as indicated by *Glossopteris* leaf impressions at Beta Peak (Fig. 2a; Capponi et al., 1999), where a 40-m-thick coal-rich succession is exposed. Field and petrographic evidence further confirm the presence of Permian strata at Ford Peak, where sandstone compositions match equivalent Permian units across Victoria Land, including the Weller Coal Measures (southern Victoria Land) and the Takrouna Formation (northern Victoria Land) (Fig. 4). At Pudding Butte, sandstones exhibiting sedimentological and compositional features consistent with Lower Triassic units occur stratigraphically above the Permian strata at Beta Peak, despite the presence of an interlayered Ferrar Dolerite sill. Similarly, the sandstones at Mount Smith (Fig. 2a), which rest directly on the crystalline basement, display compositional and stratigraphic affinities with the lowest Triassic formations, such as the Feather Conglomerate in southern Victoria Land and the Van der Hoeven Formation in northern Victoria Land (Fig. 4).

In the Ricker Hills area, Oh et al. (2019) documented a Triassic fossil-wood assemblage preserved within sandstones interpreted as braided-stream deposits, analogous to the Triassic Lashly Formation in southern Victoria Land (Collinson et al., 1983). This interpretation is consistent with our petrographic data, which reveal volcanic lithic grains in the Beacon sandstones at Ricker Hills outcrops (Fig. 4), reinforcing the correlation with the Lashly Formation (Members A, B, and C; Korsch, 1974; Collinson et al., 1983; Cornamusini et al., 2023; Zurli et al., 2024a). Sandstone at Trio Nunatak and The Mitten exhibit similar sedimentological, stratigraphic, and mineralogical characteristics reinforcing this correlation (Fig. 4). By contrast, these sandstones differ compositionally from the Lower Jurassic strata at McLea Nunatak (Bernet and Gaupp, 2005), although the mixed epiclastic and silicic–volcaniclastic Lower Jurassic deposits at McLea Nunatak resemble strata in the Convoy Range (Elliot and Grimes, 2011; Unverfärth et al., 2020). The uppermost sample from Ricker Hills (C10-15–12-12) likely corresponds to these formations. Overall, the Beacon Supergroup in the central Prince Albert Mountains comprises Permian strata, lowest Triassic strata, Lower and Middle Triassic deposits, and Upper Triassic (?) to Lower Jurassic strata (Fig. 4). The identification of Lower-Middle Triassic strata is particularly significant for correlation with southern Victoria Land (Convoy Range), especially given the absence of Triassic deposits in the adjacent portion of northern Victoria Land, where Jurassic strata rest directly on the crystalline basement. Triassic strata are, however, preserved farther north in the Victoria Land (Bomfleur et al., 2021).

6.2. Paleozoic evolution of central Prince Albert Mountains

The Paleozoic evolution of the Transantarctic Basin in the central Prince Albert Mountains is reconstructed from stratigraphic constraints and thermochronological modeling, particularly from the vertical profile at Mount Murray. This profile includes three samples at different elevations and three ZHe ages from the uppermost sample, providing the most robust thermochronological dataset in the study area. The ZHe ages exhibit a strong correlation between alpha-dose and age, indicating that age dispersion is mainly controlled by the eU concentration and supporting the reliability of applying the ZRDAAM model.

Modeled T-t paths suggest cooling of the crystalline basement during the Paleozoic at Mount Murray, reflecting an exhumation phase from the late Paleozoic to the Triassic. Although the precise onset of exhumation lies beyond the resolving power of the method, the results indicate that the basement was already being exhumed by the late Carboniferous–early Permian and had reached shallow crustal levels by the late Permian–Triassic (Fig. 5b). The modeled T-t path suggests that the basement resided at temperature around 200 °C during the early Permian (290–250 Ma), which, assuming a geothermal gradient of 25–30 °C/km, corresponds to crustal depth exceeding 5 km (Fig. 7a). This implies erosion of ~ 5 km of overburden during late Carboniferous–early Permian, uplifting and exposing basement rocks at the surface by the late Permian–Triassic. This thermal exhumation history is consistent with regional stratigraphy. Carboniferous to Permian–-Triassic exhumation aligns with the absence of upper Permian deposits

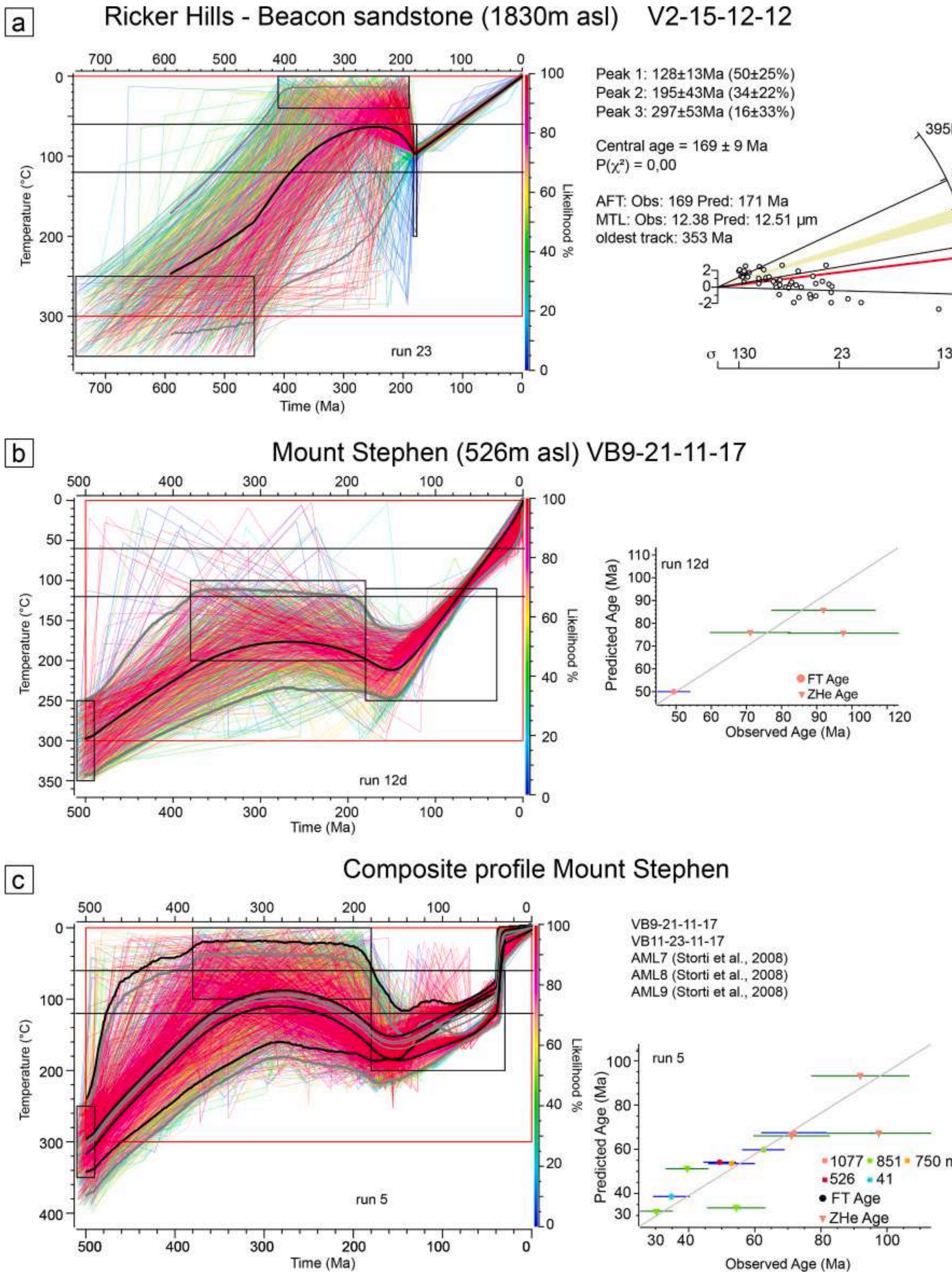

Fig. 6. Thermal history modeling result obtained from inverse and forward modeling of combined data (AFT + ZHe) using QTQt software (Gallagher, 2012) by applying the ZRDAAM for ZHe data (Guenthner et al. 2013). (a) Thermal-history paths from inverse modeling of the Beacon sample from Ricker Hills location (V2-15–12-12) based on one AFT age and track length measurement. The right panel shows a radial plot that represents the single grain age distribution with respect to the stratigraphic age and Ferrar event, showing that the samples is partially reset with some grains younger than stratigraphic age and other older. (b) Thermal-history paths from inverse modeling of the Mount Stephen sample (VB9-21–11-17) based on one AFT age, MTL and three ZHe ages. On the right, the panel shows the relationship between modeled Predicted and Observed ages where the oblique line represents the perfect match between predicted data from the modeling and the experimental data to measure the quality of modeling. (c) Thermal-history paths from inverse modeling of the composite profile of Mount Stephen-Whitmer Peninsula-Mount George Murray obtained from samples from different locations and far until 25 km. Inverse modeling used five AFT ages, four track length measurements and six single grain ZHe ages. Despite the large number of inversed data and the distance among the samples, the modeling well reproduces the observed data. On the right, the panel shows the relationship between Predicted and Observed where the oblique line represents the perfect match between predicted data from the modeling and the experimental data to measure the quality of modeling.

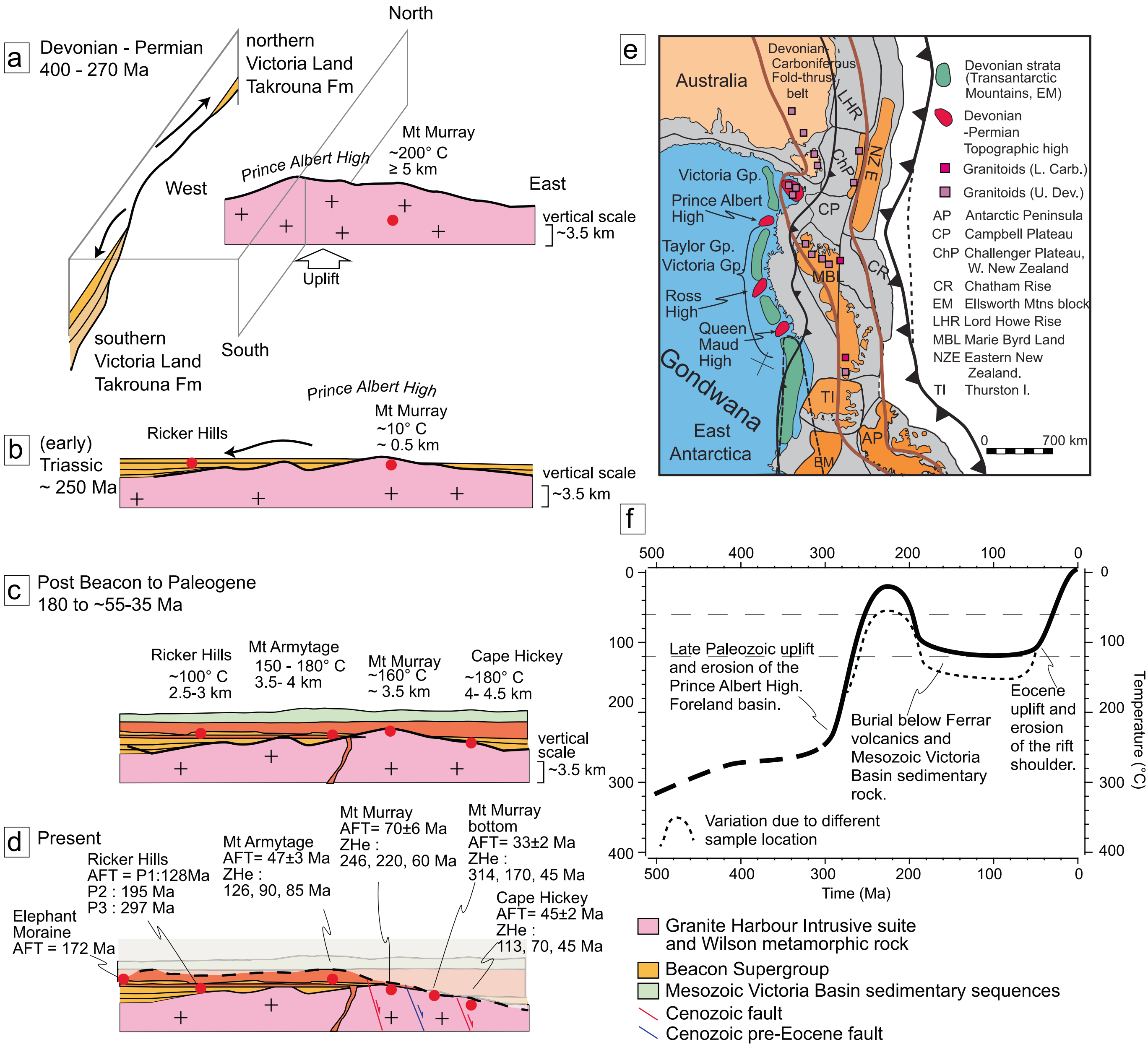

Fig. 7. Schematic diagrams showing the temporal evolution of the Prince Albert High from Devonian to the present. (a) During the Devonian to Permian, the Prince Albert High is uplifted and eroded leading the cooling of the samples from Mount Murray. Sedimentation is almost continuous in the southern Victoria Land leading the deposition of Taylor and Victoria Group, while in northern Victoria Land the sedimentation starts at late Carboniferous-early Permian (Victoria Group). (b) During the Triassic the Prince Albert High is partially or totally covered by Beacon sediments. (c) In the Mesozoic, the emplacement of Ferrar volcanic products and the sedimentation of the Mesozoic Victoria Basin led to burial and heating of the samples of the crystalline basement, of the Triassic sandstone and of the Ferrar Dolerite itself. (d) During the Cenozoic the erosion associated to rift shoulder uplift, to climatic evolution and the faulting are responsible of the present-day sample distribution. Tectonic structure that stopped before Eocene is in blue. (e) Sketch of the tectonic setting of the paleo-Pacific Gondwana margin during the Devonian to Triassic showing the occurrence of two topographic highs of the Prince Albert and Ross High. (f) Summary Temperature-time evolution of the Prince Albert High. (For interpretation of the references to colour in this figure legend, the reader is referred to the web version of this article.)

across the central Prince Albert Mountains and with the limited occurrence of Permian strata, restricted to only two localities ~ 60 km from Mount Murray. Similarly, the absence of the Taylor Group in the study area, despite its presence in the Convoy Range to the south, supports the existence of a regional topographic high. Quartzose sandstones at Mount Smith exhibit sedimentological affinities with Lower Triassic units such as the Feather Conglomerate (Cornamusini et al., 2023), consistent with the modeled T-t history indicating Permian basement erosion followed by Triassic–Early Jurassic sedimentation. We therefore propose that during deposition of the Taylor Group and lower Permian strata in southern Victoria Land, the central Prince Albert Mountains formed a topographic high, here referred to as the Prince Albert High, extending several kilometers in a north–south direction (Fig. 7a). Barrett (1981) also recognized the region corresponding to the central Prince Albert Mountains as a topographic high from the Devonian through the Triassic, proposing that it sustained ice sheets during the Late Paleozoic Ice Age; a hypothesis consistent with our reconstruction. During the early Permian, the Prince Albert High may have contributed glacially derived sediments associated with the Late Paleozoic Ice Age (Zurli et al., 2022). If this area was already exposed and elevated during this time, it is likely that portions of the landscape hosted glaciers, enhancing erosion and potentially triggering isostatic uplift, further elevating the landscape (Rolland et al., 2019; Paulsen et al., 2025).

6.3. Mesozoic evolution of the central Prince Albert Mountains

Thermal history modeling combined with stratigraphic evidence indicate that during the Triassic the basement at Mount Murray was near the surface, while fluvial sandstones were being deposited in the Ricker Hills area. Because Beacon strata at Ricker Hills did not experience post-depositional temperatures above 100 °C, their AFT ages retain partial information on sediment provenance. Older grain ages, (~380 Ma) align with the AFT ages from basement rocks that cooled between ~ 400 and 270 Ma, suggesting a shared exhumation history with Mount Murray. Petrographic data from Ricker Hills sandstones further support the contribution of local granitic sources (Fig. 7a). These observations imply that portions of the central Prince Albert Mountains remained exposed during the Triassic–Jurassic sedimentation, consistent with the absence of Beacon Supergroup strata at Mount Murray, in contrast to Mount Smith.

By the Early Jurassic (~180 Ma), Beacon Supergroup rocks were buried beneath variable thickness of Ferrar Large Igneous Province units during a regional increase in the paleogeothermal gradient (Prenzel et al., 2014, 2018) (Fig. 7c). The total present-day thickness of the Ferrar Dolerite and Kirkpatrick Basalt is estimated at ~ 1600 m (Wörner, 1992), insufficient to fully reset the AFT ages and only partially reset the ZHe ages, even under elevated geothermal gradient. Additional burial within the Mesozoic Victoria Basin likely contributed further overburden, potentially raising temperatures high enough to reset thermochronological systems. Thermal history modeling indicates that post-Beacon maximum temperatures ranged from 110 °C to 160 °C at Mount Murray and reached up to ~ 180 °C in the Mount Stephen area. Models simulating burial beneath a Mesozoic sedimentary basin at Mount Murray predict lower maximum temperatures (~110 °C), with peak heating shortly before Eocene cooling. Given uncertainties in original volcanic thickness and subsequent erosion, both scenarios remain plausible. Thermal history models reveal significant spatial variability in burial across the central Prince Albert Mountains, reflected in different degree of thermochronological resetting. At Ricker Hills, AFT were only partially reset, suggesting burial temperatures of no more than ~ 90–100 °C for the Triassic strata at Benson Knob. In contrast Mount Murray samples experienced deeper burial, leading to complete AFT resetting and partial ZHe resetting. The broad spread in ZHe ages, strongly controlled by eU content, includes some ages predating the Ferrar magmatism, further supporting heterogeneous burial and thermal histories across the region.

At Mount Murray, a maximum temperature of ~ 160 °C (in the Ferrar burial scenario; Fig. 5b) corresponds to an overburden of ~ 2.5 to 3.5 km, assuming surface temperature of 5–10 °C and geothermal gradient of 40–60 °C/km, as estimated by Prenzel et al. (2018). In the northern study area, Mount Stephen records a post-Beacon thermal event exceeding 160 °C. This temperature is significant as it potentially overcame the ZHe closure temperature, leading to age resetting. A composite profile incorporating data from Mount George Murray (Storti et al., 2008) suggests maximum heating of ~ 180 °C. Applying the paleogeothermal gradient from Prenzel et al. (2018), this temperature corresponds to burial depths of ~ 4–5 km, implying that samples from Mount Stephen and Mount George Murray were buried more deeply than those at Mount Murray. Because Beacon Supergroup strata are absent in both areas, the original vertical distance of these samples from the Kukri Erosion Surface cannot be directly constrained.

A Ferrar Dolerite sample from Mount Armytage provides one of the few thermochronological datasets from dolerites along the TAM. Both AFT and ZHe ages document a reheating phase with peak temperatures of 150–170 °C. This reheating lasted sufficiently long to produce dispersion in the ZHe age, consistent with burial beneath a sedimentary succession. Similar reheating was previously recognized in Ferrar rocks from the central Prince Albert Mountains (Molzahn et al., 1999), although their higher inferred temperatures (200–300 °C) may reflect focused hydrothermal fluid-rock interaction.

Differences between the northern and southern sectors of the study area likely reflect spatial variations in the thickness of the Mesozoic Victoria Basin, as also proposed for northern Victoria Land by Prenzel et al. (2018). For the Mount George Murray region, they estimated a combined sedimentary and volcanic thickness of approximately 3.8 km. Assuming uniform geothermal gradients, maximum temperature differences chiefly reflect variable overburden. However, spatial variations in heat flow cannot be ruled out, in which case lateral differences in geothermal gradient and not just burial depth, may explain the thermal modeling results.

6.4. Cenozoic tectonic evolution

Thermal history modeling from Mount Murray and Mount Stephen vertical profiles indicates that final exhumation began at ~ 35 Ma. This timing agrees with results from Terra Nova Bay (Prenzel et al., 2013, 2014, 2018), other regions of Victoria Land (Balestrieri et al., 2020; Olivetti et al., 2018), and the southern TAM (e.g. He et al., 2021). Along the Mount Murray profile, the uppermost sample reached temperatures of 80–90 °C during the Eocene, similar to estimates for Mount Priestley and Mount George Murray (Prenzel et al., 2018). Assuming a geothermal gradient of ~ 25 °C/km, these temperatures correspond to burial depth of ~ 3.5 km prior to final exhumation.

Comparison of thermochronological data with present-day elevation reveals a regional pattern of post-cooling vertical displacement. Eocene AFT ages from Ferrar Dolerite samples at 1,437 m and 1,159 m asl overlap with ages obtained from much lower elevation samples at Mount Stephen, Mount George Murray, and Mount Murray (526 m, 750 m, and 644 m asl, respectively). Furthermore, summits samples from Mount George Murray (71 Ma) and Mount Murray (70 Ma) yield older than the higher-elevation Ferrar samples, implying downward displacement of the latter after cooling. A similar vertical offset is observed along the coast, where AFT ages range from 35 Ma at Whitmer Peninsula to 46 Ma at Cape Hickey, despite similar elevations. These vertical inconsistencies likely reflect the geomorphological and tectonic evolution of the TAM front, which has been dissected by north–south striking Cenozoic faults (Fig. 1S; Storti and Rossetti, 2002; Storti et al., 2008; Vignaroli et al., 2015; Fioraso et al., 2025). These faults accommodated TAM uplift, segmentation of the mountain front, and subsidence of the adjacent Victoria Land Basin (e.g. Sauli et al., 2021). Recent evidence for Cenozoic faulting comes from the northern Convoy Range near Mount Murray, where fault activity associated with structurally-controlled hydrothermal fluid flow has been dated to ~ 20 Ma (Fioraso et al., 2025).

An illustrative example of this tectonic complexity is provided by four samples from the Mount Murray area (VB2, VB4, VB6-23–11-17, and the lowermost VB5-23–11-17). While the AFT ages show a consistent age-elevation relationship (Fig. 3b), the ZHe ages of the lowermost sample are old and similar to those of the uppermost sample. This apparent anomaly can be explained by fault displacement along the N–S to NE–SW–striking fault zones mapped between the lowermost and overlying samples (Fig. S1). If fault slip occurred when the samples were still buried below the Apatite Partial Annealing Zone, the relative displacement would be recorded by the zircon ZHe system but not by the AFT system. Consequently, the AFT system reflects Eocene exhumation as a single block, whereas the ZHe system retains evidence of earlier differential movements. This interpretation supports progressive fault activity beginning in the early Eocene, consistent with deformation documented in northern Victoria Land and dated between ~ 48 and 34 Ma (e.g. Di Vincenzo et al., 2004).

6.5. Implications for the tectonic evolution of the Transantarctic Basin

Late Paleozoic exhumation, inferred from thermochronological modeling and stratigraphic evidence, confirms the presence of the Prince Albert High, a major topographic high within the Transantarctic Basin. This topographic high is interpreted as analogous or potentially continuous with, the contemporaneous Ross High (Collinson et al., 1994) and Queen Maud High (Paulsen et al., 2025). Similar to the way the Ross High acted as a major morphological barrier between the Victoria Land sub-basin(s) and the central TAM basin (Fig. 1b; Collinson et al., 1994), the Prince Albert High defined the boundary between the northern and southern Victoria Land sub-basins. The influence of this primary morpho-structural divide is clearly evident in the transitional stratigraphic and compositional signatures observed across the region. The Transantarctic Basin developed between the *retro*-verging deformational front of the Gondwanide orogenic belt and the stable East Antarctic craton (Fig. 7e) (Barrett, 1981; 1991; Collinson et al., 1994; Elliot and Fleming, 2008; Goodge, 2020; Zurli et al., 2025). A recent synthesis by Paulsen et al.2025) illustrates large-scale basement exhumation across the TAM throughout the Phanerozoic, demonstrating that different segments of the TAM bedrock were exhumed/uplifted at different times, forming the basement highs that influenced the deposition of the Beacon Supergroup. Our exhumation model supports the interpretation that the Transantarctic Basin was compartmentalized into multiple sub-basins, separated by such topographic highs, which were eroded and supplied sediment to adjacent depocenters. This basin architecture is characteristic of a complex retroarc foreland system, comparable to the Cenozoic foreland basins developed along the Andean-type fold-and-thrust belts (Horton et al., 2022). Given the inferred distance between the orogenic load and basin depocenter, the Transantarctic Basin likely represents an underfilled foreland system with an erosional forebulge (e.g., Catuneanu, 2004; Horton et al., 2022). Alternating sediment sources from the orogen and the craton (Zurli et al., 2024a) further support deposition within a back-bulge basin setting (DeCelles, 2011). Analogies with the modern Andes and Gondwanide Transantarctic chain suggest that along-strike variations in foreland basin topography may have been controlled by the non-parallel geometry of the retroarc deformation front, potentially driven by non rectilinear subduction (Fig. 7e). As in the present Andean system, variable slab dip along the paleo-Pacific margin may have produced differential exhumation/uplift and subsidence within the foreland (Martinod et al., 2010; Genge et al., 2021).

In this context, uplift of the Prince Albert High may reflect far-field transmission of residual compressional stress from the paleo-Pacific convergent margin. The several-kilometer-scale exhumation inferred across a broad region is compatible with long-wavelength crustal shortening, consistent with deformation patterns associated with flat-slab subduction, similar to those proposed for the Devonian Lachlan Orogen (Collins, 2002). Additional support for flat-slab geometries along the paleo-Pacific margin during the Late Triassic–Jurassic comes from geodynamic reconstructions (Navarrete et al., 2019; Bastias et al., 2021). Collectively, these observations suggest that the Transantarctic Basin represents an ancestral broken foreland basin of Andean type (Horton et al., 2022), developed along the paleo-Pacific margin of Gondwana.

Within the studied portion of the basin, extensional tectonics likely played only a limited role in the formation of basement highs. If extension had been the dominant mechanism, it would have produced abrupt variations in sediment thickness either southward in the Convoy Range or northward in northern Prince Albert Mountains. Instead, Permian extension has been invoked primarily for the southern sectors, potentially associated with trench retreat along the paleo-Pacific margin (Rosenbaum, 2018; Paulsen et al., 2025). These insights highlight the need for further work to better resolve the tectonic drivers that governed the evolution of the Transantarctic Basin.

7. Conclusions

Thermal history modeling of AFT and ZHe data from the central Prince Albert Mountains documents a major exhumation phase spanning from the Carboniferous-early Permian to the late Permian-Triassic, that removed several kilometers of crystalline basement. Stratigraphic and petrographic analyses of the limited Beacon Supergroup exposures in the central Prince Albert Mountains show strong correlations with equivalent succession in southern Victoria Land. However, unlike in southern Victoria Land, the oldest Beacon strata in this area are late Permian to Triassic in age, with earlier units entirely absent.

The Permian exhumation and lack of lower Permian deposits support the presence of a morphological high, here referred to as the Prince Albert High. This topographic high likely formed a dome-shaped, north–south elongated topographic rise parallel to the Gondwanide deformational front, acting as a divide between the southern and northern Victoria Land sub-basins. We interpret this segmentation of the basin as the result of long-wavelength crustal shortening. This shortening was likely driven by the cratonward propagation of far-field stresses, consistent with geodynamic models that invoke flat-slab subduction of the paleo-Pacific plate during the Triassic (Navarrete et al., 2019).In this framework, the Prince Albert High represents a regional counterpart to coeval basement highs such as the Ross High and Queen Maud High in central TAM (Collinson et al., 1994; Paulsen et al., 2025).

During the Mesozoic, the region experienced burial and reheating, reaching peak temperatures of ~ 150–180 °C, equivalent to an overburden of 3–5 km depending on the assumed paleo-geothermal gradient. These thermal conditions are compatible with burial beneath the magmatic products of the Ferrar Large Igneous Province and subsequent accumulation within the Mesozoic Victoria Basin (Lisker and Läufer, 2013).

Finally, this study demonstrates that ZHe datasets characterized by large eU variability provide a powerful thermochronological tool for reconstructing thermal histories across a wide temperature range, from ~ 180 °C to below the apatite fission-track partial annealing zone, offering new insights into the long-term tectonic and erosional evolution of the Transantarctic Basin.

CRediT authorship contribution statement

Valerio Olivetti: Writing – original draft, Methodology, Investigation, Funding acquisition, Formal analysis, Data curation, Conceptualization. **Luca Zurli:** Writing – review & editing, Methodology, Formal analysis. **Silvia Cattò:** Writing – review & editing, Methodology, Formal analysis. **Fabrizio Balsamo:** Writing – review & editing, Methodology, Investigation, Data curation, Conceptualization. **Gianluca Cornamusini:** Writing – review & editing, Validation. **Marco Fioraso:** Writing – review & editing, Validation, Methodology, Formal analysis. **Matteo Perotti:** Writing – review & editing, Supervision, Methodology, Formal analysis. **Giorgia Guzzo:** Formal analysis. **Massimiliano Zattin:** Writing – review & editing, Validation, Supervision. **Federico Rossetti:** Writing – review & editing, Validation, Supervision, Investigation.

Declaration of competing interest

The authors declare that they have no known competing financial interests or personal relationships that could have appeared to influence the work reported in this paper.

Acknowledgements

This work was supported by the Italian Programma Nazionale di Ricerche in Antartide (Grant number PNRA16_00263 coordinated by V. Olivetti; PNRA_2009/A2.19 e PNRA_2013/AZ2.08 coordinated by F. Talarico; PNRA19_00120 coordinated by G. Cornamusini). We are warmly grateful for the logistics provided by the PNRA and ENEA-UTA (expedition leader: Alberto Della Rovere), and acknowledge the "Helicopters New Zealand (HNZ)" pilots and all colleagues sharing time at the Italian base "Mario Zucchelli". We thank the Museo Nazionale dell'Antartide – Siena section for operational support. VO and MZ were supported also by Geosciences Department funding (BIRD_182501). We are grateful to Giuditta Fellin and Maria Laura Balestrieri for helpful discussions. We also thank the associated editor and two anonymous reviewers, and in particular one, for their precise and rigorous revisions, which greatly improved the manuscript.

Appendix A. Supplementary data

Supplementary data to this article can be found online at https://doi.org/10.1016/j.gr.2025.12.003.

References

Balestrieri, M.L., Olivetti, V., Rossetti, F., Gautheron, C., Cattò, S., Zattin, M., 2020. Topography, structural and exhumation history of the Admiralty Mountains region, northern Victoria Land. Antarctica. Geosci. Front. 11 (5), 1841–1858.

Barrett, P.J., Grindley, G.W., Webb, P.N., 1971. The Beacon Supergroup of East Antarctica. In: Adie, R.J. (Ed.), Antarctic Geology and Geophysics: Cambridge. Cambridge University Press, UK, pp. 319–332.

Barrett, P.J., 1981. History of the Ross Sea region during the deposition of the Beacon Supergroup 400–180 million years ago. J. r. Soc. n. z. 11, 447–458. https://doi.org/10.1080/03036758.1981.10423334.

Barrett, P.J., 1991. The Devonian to Jurassic Beacon Supergroup of the Transantarctic Mountains and correlatives in other parts of Antarctica. In: Tingey, R.J. (Ed.), The Geology of Antarctica. Clarendon Press, Oxford, pp. 120–152.

Bastias, J., Spikings, R., Riley, T., Ulianov, A., Grunow, A., Chiaradia, M., Hervé, F., 2021. A revised interpretation of the Chon Aike magmatic province: active margin origin and implications for the opening of the Weddell Sea. Lithos 386–387, 106013. https://doi.org/10.1016/j.lithos.2021.106013.

Behrendt, J.C., Cooper, A., 1991. Evidence of rapid Cenozoic uplift of the shoulder escarpment of the Cenozoic West Antarctic rift system and a speculation on possible climate forcing. Geology 19, 315–319.

Bernet, M., Gaupp, R., 2005. Diagenetic history of Triassic sandstone from the Beacon Supergroup in central Victoria Land, Antarctica. New Zealand J. Geology and Geophys. 48, 447–458.

Bomfleur, B., Mörs, T., Unverfärth, J., Liu, F., Läufer, A., Castillo, P., Oh, C., Park, T.-Y.-S., Woo, J., Crispini, L., 2021. Uncharted Permian to Jurassic continental deposits in the far north of Victoria Land, East Antarctica. J. Geol. Soc. 178 (1). https://doi.org/10.1144/jgs2020-062.

Bradshaw, M.A., 2013. The Taylor Group (Beacon Supergroup): the Devonian sediments of Antarctica, in Hambrey, M. J. et al., eds., Antarctic Palaeoenvironments and Earth-Surface Processes. Geol. Soc. Lond. Spec. Publ. 381, 67–97.

Burgess, S.D., Bowring, S.A., Fleming, T.H., Elliot, D.H., 2015. High precision geochronology links the Ferrar Large Igneous Province with early Jurassic ocean anoxia and biotic crisis. Earth Planet. Sci. Lett. 415, 90–99. https://doi.org/10.1016/j.epsl.2015.01.037.

Capponi, G., Crispini, L., Meccheri, M., Musumeci, G., Pertusati, P.C., 1999. Antarctic Geological 1:250000 Map Series. Mount Joyce Quadrangle.

Capponi, G., Montomoli, C., Casale, S., Simonetti, M., 2020. Geology of the northern Convoy Range, Victoria Land. Antarctica. J. Maps 16 (2), 702–709.

Capponi, G., Montomoli, C., Simonetti, M., Salvatore, M.C., Casale, S., Musumeci, G., Cox, S., Smith Lyttle, B., Pertusati, P.C., Läufer, A., Mörs, T., 2024. A comprehensive 1: 250,000 scale geological map of the Convoy Range and Franklin Island quadrangles (Victoria Land. Antarctica). Geol. Field Trips 16 (1.5), 1–22.

Catuneanu, O., 2004. Retroarc foreland systems—evolution through time. J. African Earth Sci. 38 (3), 225–242.

Civile, D., Crispini, L., Ruppel, A., Ferrante, G.M., Morelli, D., Accettella, D., Accaino, F., Locatelli, M., Volpi, V., Busetti, M., Armadillo, E., 2025. Discovery of Cenozoic magmatic ridges and tectonics off northern Victoria Land provides new insights into the geodynamics of the Antarctic margin. Sci. Rep. 15 (1), 1–17.

Collins, W.J., 2002. Hot orogens, tectonic switching, and creation of continental crust. Geology 30 (6), 535–538.

Collinson, J.W., Pennington, D.C., Kemp, N.R., 1983. Sedimentary petrology of Permian-Triassic fluvial rocks in Allan Hills, central Victoria Land. Antarctic J. 18, 20–22.

Collinson, J.W., Pennington, D.C., Kemp, N.R., 1986. Stratigraphy and Petrology of Permian and Triassic Fluvial Deposits in Northern Victoria Land, Antarctica. In: Stump, E. (Ed.), Geological Investigations in Northern Victoria Land. American Geophysical Union (AGU). https://doi.org/10.1002/9781118664957.ch9.

Collinson, J.W., Isbell, J.L., Elliot, D.H., Miller, M.F., Miller, J.M.G., Veevers, J.J., 1994. Permian-Triassic Transantarctic basin, in: Veevers, J.J. (Ed.), Permian-Triassic Pangean Basins and Foldbelt along the Panthalassan Marfin of Gondwanaland, Geol. Soc. Am. Memoir. Veevers, J., Powell, C., Boulder, Colorado, pp. 173–222. Doi: 10.1130/MEM184-p173.

Cornamusini, G., Talarico, F.M., Cirilli, S., Spina, A., Olivetti, V., Woo, J., 2017. Upper Paleozoic glacigenic deposits of Gondwana: Stratigraphy and paleoenvironmental significance of a tillite succession in Northern Victoria Land (Antarctica). Sediment. Geol. 358, 51–69. https://doi.org/10.1016/j.sedgeo.2017.07.002.

Cornamusini, G., Zurli, L., Liberato, G.P., Corti, V., Gulbranson, E.L., Perotti, M., Sandroni, S., 2023. A lithostratigraphic reappraisal of a Permian-Triassic fluvial succession at Allan Hills (Antarctica) and implications for the terrestrial end-Permian extinction event. Palaeogeogr. Palaeoclimatol. Palaeoecol. 627, 111741. https://doi.org/10.1016/J.PALAEO.2023.111741.

DeCelles, P.G., 2011. Foreland basin systems revisited: Variations in response to tectonic settings. In Tectonics of sedimentary basins: Recent advances. Ed 405-426. Doi: 10.1002/9781444347166.ch20.

Di Giulio, A., Tribuzio, R., Ceriani, A., Riccardi, M., 1999. Integrated analyses constraining the provenance of sandstones, a case study: the Section Peak Formation (Beacon Supergroup, Antarctica). Sediment. Geol. 124, 169–183. https://doi.org/10.1016/S0037-0738(98)00126-2.

Di Vincenzo, G., Rocchi, S., Rossetti, F., Storti, F., 2004. 40Ar–39Ar dating of pseudotachylytes: the effect of clast-hosted extraneous argon in Cenozoic fault-generated friction melts from the West Antarctic Rift System. Earth Planet. Sci. Lett. 223 (3–4), 349–364.

Elliot, D.H., 1992. Jurassic Magmatism and the Causes of the Breakup of Gondwana. Geol. Soc. Lond., Spec. Publ. 68 (1), 107–124.

Elliot, D.H., 1996. The Hanson Formation: a new stratigraphical unit in the Transantarctic Mountains. Antarctica. Antarctic Sci. 8, 389–394.

Elliot, D.H., Fleming, T.H., 2008. Physical volcanology and geological relationships of the Jurassic Ferrar large Igneous Province. Antarctica. J. Volcanology and Geothermal Res. 172, 20–37.

Elliot, D.H., Grimes, C.G., 2011. Triassic and Jurassic strata at Coombs Hills, south Victoria Land: stratigraphy, petrology and cross-cutting breccia pipes. Antarctic Sci. 23 (3), 268–280.

Elliot, D.H., 2013. The geological and tectonic evolution of the Transantarctic Mountains: a review: in Hambrey, M. J., Barker, P. F., Barrett, P. J., Bowman, V., Davies, B., Smellie, J. L., Tranter, M. (eds), Antarctic Palaeoenvironments and Earth-Surface Processes. Geol. Soc. Lond. Spec. Publ. 381, 7–35.

Elliot, D.H., Fanning, C.M., Hulett, S.R.W., 2015. Age provinces in the Antarctic craton: evidence from detrital zircons in Permian strata from the Beardmore Glacier region. Antarctica. Gondwana Res. 28, 152–164.

Elliot, D.H., Fanning, C.M., Isbell, J.L., Hulett, S.R.W., 2017. The Permo-Triassic Gondwana sequence, central Transantarctic Mountains, Antarctica: Zircon geochronology, provenance, and basin evolution. Geosphere 13, 155–178. https://doi.org/10.1130/GES01345.1.

Elliot, D.H., Fanning, C.M., Mukasa, S.B., Millar, I.L., 2019. Hf- and O-isotope data from detrital and granitoid zircons reveal characteristics of the Permian–Triassic magmatic belt along the Antarctic sector of Gondwana. Geosphere 15, 576–604. https://doi.org/10.1130/GES02011.1.

Elliot, D.H., White, J.D.L., Fleming, T.H., 2021. Ferrar Large Igneous Province: volcanology, Volcanism in Antarctica: 200 Million Years of Subduction. Smellie, K. S. Panter, A. Geyer, Rifting and Continental Break-up, J. L.

Elliot, D.H., Fleming, T.H., 2021. Ferrar Large Igneous Province: petrology, Volcanism in Antarctica: 200 Million Years of Subduction. Smellie, K. S. Panter, A. Geyer, Rifting and Continental Break-up, J. L.

Encarnación, J., Fleming, T.H., Elliot, D.H., Eales, J.V., 1996. Synchronous emplacement of Ferrar and Karoo dolerites and the early breakup of Gondwana. Geology 24, 535–538.

Fioraso, M., Olivetti, V., Balsamo, F., Rossetti, F., Zattin, M., Cornamusini, G., 2025. Cenozoic structurally controlled hydrothermal activity revealed by apatite thermochronology in the Convoy Range (southern Victoria Land. Antarctica). Geochem, Geophys, Geosyst. 26 (4), 2024GC012005.

Fitzgerald, P.G., 1992. The Transantarctic Mountains of southern Victoria Land: the application of apatite fission track analysis to a rift shoulder uplift. Tectonics 11, 634–662.

Fitzgerald, P.G., 2002. Tectonics and landscape evolution of the Antarctic plate since the breakup of Gondwana, with an emphasis on the West Antarctic Rift System and the Transantarctic Mountains. R. Soc. n. z. Bull. 35, 453–469.

Fitzgerald, P.G., Baldwin, S.L., Webb, L.E., O'Sullivan, P.B., 2006. Interpretation of (U-Th)/He single grain ages from slowly cooled crustal terranes: a case study from the Transantarctic Mountains of southern Victoria Land. Chem. Geol. 225, 91–120. https://doi.org/10.1016/j.chemgeo.2005.09.001.

Gallagher, K., 2012. Transdimensional inverse thermal history modeling for quantitative thermochronology. J. Geophys. Res. 117, B02408. https://doi.org/10.1029/2011JB008825.

Gazzi, P., 1966. Mineral. Petrogrographica Acta 12, 69–97.

Genge, M.C., Zattin, M., Savignano, E., Franchini, M., Gautheron, C., Ramos, V.A., Mazzoli, S., 2021. The role of slab geometry in the exhumation of cordilleran-type orogens and their forelands: Insights from northern Patagonia. Geol. Soc. Am. Bull. 133 (11–12), 2535–2548.

Gérard, B., Robert, X., Grujic, D., Gautheron, C., Audin, L., Bernet, M., Balvay, M., 2022. Zircon (U-Th)/He closure temperature lower than apatite thermochronometric systems: Reconciliation of a paradox. Minerals 12 (2), 145.

Glen, R.A., Cooper, R.A., 2021. Evolution of the East Gondwana convergent margin in Antarctica, southern Australia and New Zealand from the Neoproterozoic to latest Devonian. Earth-Sci. Rev. 220, 103687.

Goodge, J.W., 2002, From Rodinia to Gondwana: Supercontinent evolution in the Transantarctic Mountains, in Gamble, J.A., Skinner, D.N.B., and Henrys, S., eds., Proceedings of the 8th International Symposium on Antarctic Earth Sciences: Royal Soc. N. Zeal. Bul., v. 35, p. 61–74.

Goodge, J.W., 2020. Geological and tectonic evolution of the Transantarctic Mountains, from ancient craton to recent enigma. Gondwana Res. 80, 50–122. https://doi.org/10.1016/j.gr.2019.11.001.

Guenthner, W.R., Reiners, P.W., Ketcham, R.A., Nasdala, L., Giester, G., 2013. Helium diffusion in natural zircon: Radiation damage, anisotropy, and the interpretation of zircon (U-Th)/He thermochronology. Am. J. Sci. 313 (3), 145–198.

Guenthner, W.R., Reiners, P.W., Tian, Y., 2014. Interpreting date–eU correlations in zircon (U-Th)/He datasets: a case study from the Longmen Shan. China. Earth Planet. Sci. Lett. 403, 328–339.
Guenthner, W.R., Reiners, P.W., Drake, H., Tillberg, M., 2017. Zircon, titanite, and apatite (U-Th)/He ages and age-eU correlations from the Fennoscandian Shield, southern Sweden. Tectonics 36 (7), 1254–1274.
Gunn, B.M., Warren, G., 1962. Geology of Victoria Land between the Mawson and Mulock glaciers, Antarctica. New Zealand Geol. Surv, Bull, p. 71.
Harrington. J., 1965. Geology and morphology of Antarctica. In Van Oye, P. & Van Mieghen J., eds. Biogeography and ecology in Antarctica. Monographiae Biologiciae, 15, 1-7 1.
Härtel, B., Jonckheere, R., Krause, J., Ratschbacher, L., 2022. Spurious age-eU associations in thermochronological data. Earth Planet. Sci. Lett. 599, 117870.
Härtel, B., Enkelmann, E., 2024. The daughter-parent plot: a tool for analyzing thermochronological data. Geochronology Discussions 2024, 1–28.
He, J., Thomson, S.N., Reiners, P.W., Hemming, S.R., Licht, K.J., 2021. Rapid erosion of the central Transantarctic Mountains at the Eocene-Oligocene transition: evidence from skewed (U-Th)/He date distributions near Beardmore Glacier. Earth Planet. Sci. Lett. 567, 117009.
Hurford, A.J., 1990. International Union of Geological Sciences Subcommission on Geochronology recommendation for the standardization of fission track dating calibration and data reporting. Nucl. Tracks 17, 233–236.
Hurford, A.J., Green, P.F., 1983. The zeta age calibration of fission track dating. Chem. Geol. 1, 285–317.
Horton, B.K., Capaldi, T.N., Mackaman-Lofland, C., Perez, N.D., Bush, M.A., Fuentes, F., Constenius, K.N., 2022. Broken foreland basins and the influence of subduction dynamics, tectonic inheritance, and mechanical triggers. Earth-Sci. Rev. 234, 104193.
Koch, Z.J., Isbell, J.L., 2013. Processes and products of grounding-line fans from the Permian Pagoda Formation, Antarctica: Insight into glacigenic conditions in polar Gondwana. Gondwana Res. 24, 161–172. https://doi.org/10.1016/j.gr.2012.10.005.
Kyle, R.A., 1977. Palynostratigraphy of the Victoria Group of South Victoria Land. Antarctica. n. Zeal. J. Geol. Geophys. 20 (6), 1081–1102.
Ingersoll, R.V., Bullard, T.F., Ford, R.L., Grimm, J.P., Pickle, J.D., Sares, S.W., 1984. The effect of grain size on detrital modes: a test of the Gazzi-Dickinson point-counting method. J. Sediment. Res. 54, 103–116. https://doi.org/10.1306/212F83B9-2B24-11D7-8648000102C1865D.
Isbell, J.L., 1999. The Kukri erosion Surface: a reassessment of its relationship to rocks of the Beacon Supergroup in the central Transantarctic Mountains. Antarctica. Antarctic Sci. 11, 228–238.
Isbell, J.L., Koch, Z.J., Szablewski, G.M., Lenaker, P.A., 2008. In: Permian Glacigenic Deposits in the Transantarctic Mountains, Antarctica. https://doi.org/10.1130/2008.2441(04).
Isbell, J.L., Henry, L.C., Gulbranson, E.L., Limarino, C.O., Fraiser, M.L., Koch, Z.J., Ciccioli, P.L., Dineen, A.A., 2012. Glacial paradoxes during the late Paleozoic ice age: evaluating the equilibrium line altitude as a control on glaciation. Gondwana Res. 22, 1–19.
Jordan, T.A., Riley, T.R., Siddoway, C.S., 2020. The geological history and evolution of West Antarctica. Nature Rev. Earth & Environment 1 (2), 117–133.
Ketcham, R.A., Carter, A., Donelick, R.A., Barbarand, J., Hurford, A.J., 2007. Improved modeling of fission-track annealing in apatite. Am. Mineralogist 92 (5–6), 799–810.
Korsch, R.J., 1974. Petrographic comparison of the Taylor and Victoria groups (Devonian to Triassic) in South Victoria Land. Antarctica. New Zeal. J. Geol. Geophys. 17, 523–541. https://doi.org/10.1080/00288306.1973.10421579.
Lisker, F., 2002. Review of FT studies in northern Victoria Land – passive margin evolution versus uplift of the Transantarctic Mountains. Tectonophysics 349, 57–73.
Lisker, F., Läufer, A.L., 2013. The Mesozoic Victoria Basin: Vanished link between Antarctica and Australia. Geology 41 (10), 1043–1046.
Lisker, F., Läufer, A., Rossetti, F., Olesch, M., Schäfer, T., 2006. The Transantarctic Beacon Basin: new insights from FT data and structural data from the USARP Mountains and adjacent areas (northern Victoria Land, Antarctica). Basin Res. 18, 315–340.
Martinod, J., Husson, L., Roperch, P., Guillaume, B., Espurt, N., 2010. Horizontal subduction zones, convergence velocity and the building of the Andes: Earth Planet. Sci. Lett. 299, 299–309. https://doi.org/10.1016/j.epsl.2010.09.010.
McKelvey, B.C., Webb, P.N., Gorton, M.P., Kohn, B.P., 1970. Stratigraphy of the Beacon Supergroup between the Olympus and Boomerang ranges. Victoria Land: Nature 227, 1126–1128.
McKelvey, B.C., Webb, P.N., Kohn, B.P., 1977. Stratigraphy of the 853 Taylor and lower Victoria groups (Beacon Supergroup) between the Mackay Glacier and Boomerang Range. Antarctica. New Zeal. J. Geol. Geophys. 20, 813–863. https://doi.org/10.1080/00288306.1977.10420685.
Miller, S.R., Fitzgerald, P.G., Baldwin, S.L., 2010. Cenozoic range-front faulting and development of the Transantarctic Mountains near Cape Surprise, Antarctica: thermochronologic and geomorphologic constraints. Tectonics 29 (1).
Molzahn, M., Wörner, G., Henjes-Kunst, F., Rocholl, A., 1999. Constraints on the cretaceous thermal event in the Transantarctic Mountains from alteration processes in Ferrar flood basalts. Global and Planetary Change 23, 45–60.
Navarrete, C., Gianni, G., Encinas, A., Marquez, M., Kamerbeek, Y., Valle, M., Folguera, A., 2019. Triassic to Middle Jurassic geodynamic evolution of southwestern Gondwana: from a large flat-slab to mantle plume suction in a rollback subduction setting. Earth Sci. Rev. 194, 125–129. https://doi.org/10.1016/j.earscirev.2019.05.002.
Oh, C., Lee, J.H., Woo, J., Lee, J.I., 2019. New occurrence of Triassic gymnosperm wood at the Ricker Hills, southern Victoria Land, Antarctica: Rev. Palaeobot. Palynol. 261, 95–102. https://doi.org/10.1016/j.revpalbo.2018.11.006.
Olivetti, V., Rossetti, F., Balestrieri, M.L., Pace, D., Cornamusini, G., Talarico, F., 2018. Variability in uplift, exhumation and crustal deformation along the Transantarctic Mountains front in southern Victoria Land, Antarctica. Tectonophysics 745, 229–244.
Paulsen, T., Benowitz, J., Thomson, S., Encarnacion, J., Grunow, A., Layer, P., Young, M., 2025. Antarctic Phanerozoic landscape evolution along the Transantarctic basin from thermochronology. Earth Planet. Sci. Lett. 664, 119445.
Prenzel, J., Lisker, F., Balestrieri, M.L., Läufer, A., Spiegel, C., 2013. The Eisenhower Range, Transantarctic Mountains: Evaluation of qualitative interpretation concepts of thermochronological data. Chem.he Geol. 352, 176–187.
Prenzel, J., Lisker, F., Elsner, M., Schöner, R., Balestrieri, M.L., Läufer, A.L., Berner, U., Spiegel, C., 2014. Burial and exhumation of the Eisenhower Range, Transantarctic Mountains, based on thermochronological, sedimentary rock maturity and petrographic constraints. Tectonophysics 630, 113–130.
Prenzel, J., Lisker, F., Monsees, N., Balestrieri, M.L., Läufer, A., Spiegel, C., 2018. Development and inversion of the Mesozoic Victoria Basin in the Terra Nova Bay (Transantarctic Mountains) derived from thermochronological data. Gondwana Res. 53, 110–128.
Reiners, P.W., Farley, K.A., Hickes, H.J., 2002. He diffusion and (U-Th)/He thermochronometry of zircon: initial results from fish Canyon Tuff and Gold Butte. Tectonophysics 349 (1–4), 297–308. https://doi.org/10.1016/S0040-1951(02)00058-6.
Rocchi, S., Tonarini, S., Armienti, P., Innocenti, F., Manetti, P., 1998. Geochemical and isotopic structure of the early Palaeozoic active margin of Gondwana in northern Victoria Land, Antarctica. Tectonophysics 284, 261–281. https://doi.org/10.1016/S0040-1951(97)00178-9.
Rolland, Y., Bernet, M., van der Beek, P., Gautheron, C., Duclaux, G., Bascou, J., Balvay, M., Héraudet, L., Sue, C., Ménot, R.P., 2019. Late Paleozoic Ice Age glaciers shaped East Antarctica landscape. Earth Planet. Sci. Lett. 506, 123–133.
Rosenbaum, G., 2018. The Tasmanides: Phanerozoic tectonic evolution of Eastern Australia. Annu. Rev. Earth Planet. Sci. 46, 291–325.
Rossetti, F., Lisker, F., Storti, F., Läufer, A.L., 2003. Tectonic and denudational history of the Rennick Graben (North Victoria Land): Implications for the evolution of rifting between East and West Antarctica. Tectonics 22 (2).
Rossetti, F., Storti, F., Busetti, M., Lisker, F., Di Vincenzo, G., Läufer, A., Rocchi, S., Salvini, F., 2006. Eocene initiation of Ross Sea dextral faulting and implications for East Antarctic neotectonics. J. Geol. Soc. 163, 119–126.
Sauli, C., Sorlien, C., Busetti, M., De Santis, L., Geletti, R., Wardell, N., Luyendyk, B.P., 2021. Neogene Development of the terror Rift, Western Ross Sea. Antarctica. Geochem. Geophys. Geosystems 22. https://doi.org/10.1029/2020GC009076.
Siddoway, C.S., Baldwin, S.L., Fitzgerald, P.G., Fanning, C.M., Luyendyk, B.P., 2004. Ross Sea mylonites and the timing of intracontinental extension within the West Antarctic rift system. Geology 32 (1), 57–60.
Siddoway, C.S., 2008. Tectonics of the West Antarctic Rift System: new light on the history and dynamics of distributed intracontinental extension. A keystone in a changing world, Antarctica, pp. 91–114.
Schöner, R., Viereck-Götte, L., Schneider, J., Bomfleur, B., 2007, Triassic-Jurassic sediments and multiple volcanic events in North Victoria Land, Antarctica: A revised stratigraphic model: in Cooper, A. K., Raymond, C. R. et al., eds., Antarctica: A Keystone in a Changing World, National Academies Press, Washington, DC, 5 pp. doi:https://doi.org/10.3133/of2007-1047.srp102.
Storti, F., Rossetti, F., 2002. Brittle deformation of the Beacon and Ferrar rocks in the Eisenhower Range-deep Freeze Range area, northern Victoria Land, Antarctica. Terra Antartica 9, 19–28.
Storti, F., Salvini, F., Rossetti, F., Morgan, J.P., 2007. Intraplate termination of transform faulting within the Antarctic continent. Earth Planet. Sci. Lett. 260 (1–2), 115–126.
Storti, F., Balestrieri, M.L., Balsamo, F., Rossetti, F., 2008. Structural and thermochronological constraints to the evolution of the West Antarctic Rift System in central Victoria Land. Tectonics 27 (4).
Stump, E., 1992. The Ross Orogen of the Transantarctic Mountains in the light of the Laurentia-Gondwana split. GSA Today 2, 25–28.
Stump, E., 1995. The Ross orogen of the Transantarctic Mountains. Cambridge University Press, Cambridge.
Sugden, D.E., Denton, G.H., Marchant, D.R., 1995. Landscape evolution of the Dry Valleys, Transantarctic Mountains: tectonic implications. J. Geophys. Res. Solid Earth 100 (B6), 9949–9967.
Sugden, D.E., Denton, G.H., 2004. Cenozoic landscape evolution of the Convoy Range to Mackay Glacier area, Transantarctic Mountains: Onshore to offshore synthesis. Geol. Soc. Am. Bull. 116 (7–8), 840–857. https://doi.org/10.1130/B25356.1.
Unverfärth, J., Mörs, T., Bomfleur, B., 2020. Palynological evidence supporting widespread synchronicity of Early Jurassic silicic volcanism throughout the Transantarctic Basin. Antarct. Sci. 32, 396–397. https://doi.org/10.1017/S0954102020000346.
Veevers, J.J., 2004. Gondwanaland from 650–500Ma assembly through 320 Ma merger in Pangea to 185–100 Ma breakup: supercontinental tectonics via stratigraphy and radiometric dating. Earth-Sci. Rev. 68, 1–132.
Vignaroli, G., Balsamo, F., Giordano, G., Rossetti, F., Storti, F., 2015. Miocene-to-Quaternary oblique rifting signature in the Western Ross Sea from fault patterns in the McMurdo Volcanic Group, north Victoria Land, Antarctica. Tectonophysics 656, 74–90.
Walker, B.C., 1980. The petrology of the Triassic strata at Horseshoe Mountain, South Victoria Land. Victoria University of Wellington, Antarctica.

Wolfe, M.R., Stockli, D.F., 2010. Zircon (U-Th)/He thermochronometry in the KTB drill hole, Germany, and its implications for bulk He diffusion kinetics in zircon. Earth Planet. Sci. Lett. 295 (1–2), 69–82. https://doi.org/10.1016/j.epsl.2010.03.025.

Wörner, G., 1992. Kirkpatrick Lavas, Exposure Hill Formation and Ferrar Sills in the Prince Albert Mountains, Victoria Land. Antarctica. Polarforschung 60 (2), 87–90.

Zurli, L., Cornamusini, G., Woo, J., Liberato, G.P., Han, S., Kim, Y., Talarico, F.M., 2022. Detrital zircons from late Paleozoic Ice Age sequences in Victoria Land (Antarctica): New constraints on the glaciation of southern Gondwana. Geol. Soc. Am. Bull. 134 (1–2), 160–178.

Zurli, L., Liberato, G.P., Perotti, M., Woo, J., Lee, M.J., Cornamusini, G., 2024a. A multi-proxy detrital study from Permian-Triassic fluvial sequences of Victoria Land (Antarctica): Implications for the Gondwanan basin evolution. Palaeogeogr. Palaeoclimatol Palaeoecol 112–113. https://doi.org/10.1016/j.palaeo.2024.112113.

Zurli, L., Perotti, M., Cornamusini, G., 2024b. Composition of late Paleozoic Ice Age tillites in Victoria Land (Antarctica): implications for sediment provenance and ice centers extent in southern Gondwana. Rendiconti Online Soc. Geol. It. 63, 1–8. https://doi.org/10.3301/ROL.2024.27.

Zurli, L., Fioraso, M., Perotti, M., Di Giulio, A., Olivetti, O., Pezzoli, S., Corti, V., Cornamusini, G., 2025. Evolution of the Transantarctic Basin (southern Gondwana): insights from quantitative sandstone petrography. N. Zeal. J. Geol. Geophys.

Barrett, P.J., Elliot, D.H., and Lindsay, J.F., 1986, The Beacon Supergroup (Devonian–Triassic) and Ferrar Group (Jurassic) in the Beardmore Glacier area, Antarctica, in Turner, M.D., and Splettstoesser, J.F., eds., Geology of the Central Transantarctic Mountains: American Geophysical Union, Antarctic Research Series 36, 339–428, DOI: 10.1029/AR036p0339.

Fioraso, M., Sternai, P., Olivetti, V., Balestrieri, M.L., Zattin, M., Cornamusini, G., 2024. Miocene climate cooling and aridification of Antarctica may have enhanced syn-extensional magmatism in the western Ross Sea. Global and Planet. Chan. 240, 104538.